Computer Aided Diagnosis on customized Ultrasound Imaging system

Vivek Akkala

A Thesis Submitted to

Indian Institute of Technology Hyderabad

In Partial Fulfillment of the Requirements for

The Degree of Master of Technology

Department of Electrical Engineering

June 2015

Declaration

I declare that this written submission represents my ideas in my own words, and where ideas or words of others have been included, I have adequately cited and referenced the original sources. I also declare that I have adhered to all principles of academic honesty and integrity and have not misrepresented or fabricated or falsified any idea/data/fact/source in my submission. I understand that any violation of the above will be a cause for disciplinary action by the Institute and can also evoke penal action from the sources that have thus not been properly cited, or from whom proper permission has not been taken when needed.

(Signature)

Vivek Akkala
EE12M1041
(Roll No.)

Approval Sheet

This Thesis entitled Computer Aided Diagnosis on customized Ultrasound Imaging system by Vivek Akkala is approved for the degree of Master of Technology from IIT Hyderabad

(Dr. Sumohana Channappayya) Examiner
Department of Electrical Engineering
IIT Hyderabad

(Dr. Ch. Sobhan Babu) Examiner
Department of Computer Science and Engineering
IIT Hyderabad

(Dr. P. Rajalakshmi) Adviser
Department of Electrical Engineering
IIT Hyderabad

Acknowledgements

I sincerely express my gratitude to everyone who supported me throughout the course of this work. I am thankful to my advisor Dr. P. Rajalakshmi for her aspiring guidance, invaluably constructive criticism and friendly advice during the work. I am also thankful to Dr. Sumohana Channappayya, Dept. of Electrical Engineering for his guidance on several issues related to the project.

A significant part of this thesis was benefited from the discussions that took place in the half yearly meetings of IU-ATC project that is aimed at Centre Of Excellence in Next Generation Networks, Systems and Services. I am thankful to all the participants of those meetings, especially Dr. Uday B Desai, Dr. Ashok Jhunjhunwala who attended the presentations and shared their views from time to time.

I am also thankful to my friends at IIT Hyderabad. Although it is not possible to mention all of them, R. Bharath and Harsha Ponduri deserve a special mention for the enormous amount of help they have provided.

Finally, I thank Dr. Abdul Mateen Mohammed, Asian Institute of Gastroentrology, for the discussion related to diagnosis of kidney.

Dedication

To my family and to everyone who has been part of my learning experiences.

Abstract

This thesis seeks implementation of midend, backend algorithms to develop ultrasound imaging system and computer aided diagnosis for kidney. Integration of new algorithms onto present ultrasound system is not possible as they are mostly based on DSPs and FPGAs. Hence firstly, midend and backend system has been designed for Kintex 7 FPGA, to replicate present ultrasound system. Later our algorithms related to compression techniques, image contrast enhancement are validated by porting them on to the developed system. The thesis also focuses on diagnosing kidney related problems using ultrasound images. Recent statistics show that there is a large increase in population suffering with kidney related problems. Many a times, detecting the kidney related problem at an early stage can prevent most of these diseases. Some of the major issues in maintaining quality of healthcare services are low doctor to patient ratio in rural areas, unavailability of trained medical professionals in remote areas, infrastructural constraints etc. Computer aided diagnosis helps in solving this issue. Computer aided algorithms can assist semi-skilled sonographers to confidently make decisions, thus improving the quality of healthcare services.

In order to realize an ultrasound system and computer aided diagnosis, several engineering aspects need attention. The signal processing algorithms related to midend and backend design of ultrasound system include envelope detection, compression techniques to fit dynamic range and image enhancement techniques to obtain good quality image. From the results obtained, it is observed that rather than log compression used in most of the ultrasound machines, gamma compression best suites ultrasound system for compressing the signals obtained from transducer. Further image processing algorithms like Viola Jones algorithm, Genetic algorithm are used to segment kidney and extract the features of kidney, that aids in determining whether kidney is normal or not.

The backend ultrasound system along with computer aided diagnosis is implemented successfully on FPGAs available in market like Kintex 7 and Zed board. Computer aided diagnosis algorithms are validated on the designed system with a good accuracy.

Contents

Chapter 1

Introduction

Medical images can be diagnosed through various imaging modalities like Magnetic Resonance Imaging (MRI), Computed Tomography (CT), Ultrasonography (US), Intravenous Urography (IVU), Angiography (AG). Each of this modality has distinct advantages and disadvantages in contrast formation, sensitivity, resolution, level of invasive and cost. MRI gives the same information as CT scan in regards to kidney imaging. However, the contrast material gadolinium present in MRI is associated with Nephrogenic Systemic Fibrosis (NSF) [1], which decreases the kidney functioning. IVU is used to measure kidney size, shape and in the evaluation of pelvis and ureters. The major drawback with IVU technique is, due to radiation and IV contrast administration there may be renal failures [2]. CT uses computer processed X-rays to form tomographic image and gives most of the details similar to ultrasound. But this has disadvantage of radiation exposure and also usage of contrast dye can cause kidney damage. Ultrasound-based diagnostic imaging technique is used for visualizing body structures and is called ultrasonography. Ultrasonography is an ultrasound based imaging technique for visualizing internal organs structure, at real time. It uses ultrasound spectrum from 1MHz to 50MHz for good resolution and good penetrating ability [3]. These ultrasound signals are generated by converting a Radio Frequency (RF) electrical signal into mechanical vibration via a piezoelectric transducer sensor [4]. Ultrasonography interprets the echoes of high frequency sound waves sent into the biological tissue from the surface and forms the image. It is used for both diagnosis and therapeutic procedures with least invasive as it is radiation free, patient-friendly and less expensive when compared to other procedures [5].

The developing trend in the digital electronics lead to the development in the ultrasound systems particularly in improving the image quality and decreasing the price for implementation. Traditional ultrasound machines are not very flexible in implementing new features as they were built using multiple fixed-function circuit boards to meet high data rate requirements [6]. Design of ultrasound machines in the recent years could provide some flexibility in core ultrasound processing by using FPGAs. Digital processing techniques on Field Programmable Gate Array (FPGA) based ultrasound system, gives better flexibility over traditional microprocessors and DSPs in implementation of new algorithms because of their re-configurable characteristics. This use of modern components and the flexible modular architecture has prepared the platform for adaptation to new signal-processing technologies [7], [8], [9]. This allows researchers to explore various computing platforms to implement ultrasound signal processing algorithms to extend the uses of ultrasound machines. The FPGA

configuration is generally specified using a hardware description language (HDL). FPGAs contain programmable logic components called logic blocks that can be configured to perform complex computational functions [10]. Implementation on FPGA can miniaturize the traditional ultrasound machines. It provides high performance platform for realization of application specific ultrasound instruments and many image processing capabilities at low cost, thereby decreasing the cost of patient diagnosis. The compact design with high image quality is a very good solution to improve the health care level specifically in rural areas.

In this thesis, we focused on FPGA implementation of the backend processing for ultrasound system. Backend processing consists of Hilbert transform to extract the envelope of signal received from analog front end, compression technique to extract image information from the envelope and reduce the dynamic range. Later scan conversion is applied to display the B-mode image of the tissue structure by converting the pulse echo from polar form (r,θ) to Cartesian form. Finally full scale contrast stretch image enhancement technique is implemented to improve the image contrast.

Kidneys help in controlling chemical composition of fluids in the tissue and blood by removing wastes. They maintain proper concentration of nutrients and ions in the body by regulating amount of water in blood [11]. According to Indian council of medical research (ICMR), it is estimated that 77.2 million people are suffering from pre-diabetes, a condition in which the patients have high blood glucose level which is not in diabetes range but having great risk of getting diabetes. Out of 1.27 billion population 65.1 million patients are confirmed diabetes and 17 million diabetes patients are suffering from several other kidney problems like cyst and stone. Delay in treatment for these disorders can lead to damage in nephrons, accumulation of water and toxic wastes in the body. Hence these problems are to be diagnosed immediately. So there is a need to design a system for preliminary diagnosis of kidney diseases, which should be portable and operator independent. The potentiality of portable ultrasound scanning in point of care applications and remote diagnosis is limited due to lack of sonographers. As per Rural Health Statistics in India 2012, there is a requirement of 4833 sonographers at Community Health Centres (CHC) where only 2314 sonographers positions (less than 50%) are filled [12], in these sort of circumstances, semi-skilled persons can diagnose the patients with the help of computer aided diagnosis (CAD). CAD is termed as diagnosing the patients automatically without manual intervention.

Accurate detection of abnormalities in kidney is very beneficial for patients to get early treatment. In this thesis, we focused on detecting abnormalities like cyst and stones in kidney by analyzing ultrasound videos. The stones and cysts in ultrasound image are identified in following way: The stones in kidney appear bright compared to neighbor region due to strong reflections from the stone. The cyst in kidney has low reflectivity to sound and appears as dark region in kidney. The cyst and stone in ultrasound images are shown in Fig. 1.1. The structure of kidney varies, so its a challenging task to localize the kidney in ultrasound images. These variations depends on physical appearance of a person like height, weight etc., The size of kidney also varies with diseases like diabetes, cysts. Sometimes, the full part of kidney is not observed due to occlusions from other organs. kidney is made up of soft tissues, relative position of person with transducer can affect shape of kidney. Due to above factors, shape and size of kidney is going to be highly diversified and is not easy to come up with kidney localization techniques.

Here, algorithm is proposed to automatically diagnose kidney by analyzing ultrasound videos. Initially ultrasound video of kidney is converted into frames. From each sampled frame, we look for

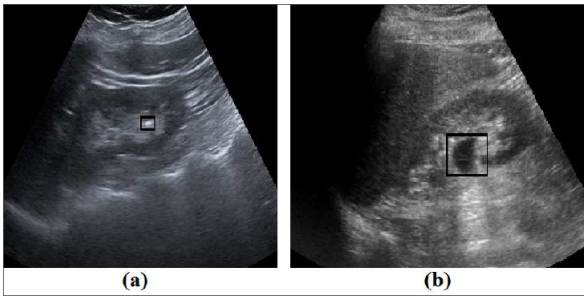

Figure 1.1: Rectangular box show the abnormalities present in kidney (a) stone. (b) cyst.

the presence of kidney using Viola Jones algorithm (machine learning algorithm). After detecting the kidney in an image, then its textural features are extracted from the detected part of kidney and are fed to supervised classifier which is pre-trained with textural features of normal and abnormal kidney. All the texture features may not be useful in classifying the image. A Genetic algorithm is used to find the effective features of kidney and only these features are used for training the SVM classifier. Computing the effective features reduces the computation time, making our proposed algorithms feasible to use in real time applications. The trained classifier will classify the image based on its features. The same algorithm is repeated for all frames present in the video. The abstract level representation of proposed algorithm is shown in Fig. 1.2. The novelties proposed in the paper are: The frame selector, which selects the frames in video for diagnosing. Viola Jones algorithm is used for detecting the kidneys, which is robust with respect to shape, size and orientations. No assumptions are made regarding data acquisition, which is significant contribution for detecting the kidney.

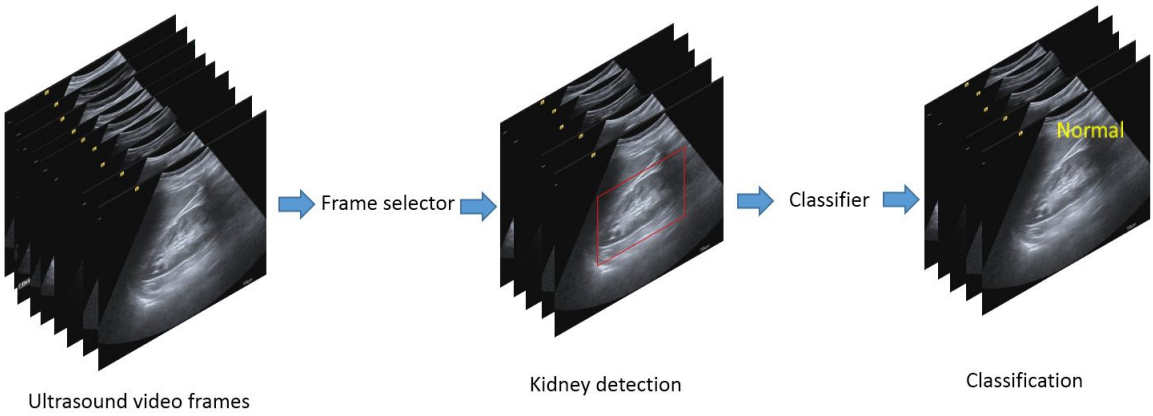

Figure 1.2: Abstract level representation of proposed algorithm for diagnosing kidney.

1.1 Literature Survey

Previously, the programmable ultrasound system architecture was proposed, in which digital signal processors (DSPs) are used for performing core ultrasound signal and image processing [13], [14]. Because of improved flexibility and efficiency, the programmable ultrasound system can quickly test new clinical imaging modes and algorithms [15][17]. In addition, the programmable approach

has been evaluated for POC diagnostic imaging systems, especially computational capabilities [18], [19]. However, these evaluations were inconclusive because they were conducted with commercially available testing boards, instead of building a prototypical device.

Computer Aided Diagnosis (CAD) has become one of the major tools for medical imaging and diagnostic radiology. Medical diagnostics are highly biased to the person skill and mood. Computer assisted diagnosis can be very handy and will significantly improve the decision making without human intervention. CAD is used to provide a computer output as a second opinion to assist radiologists image interpretation and reducing the time for reading the image. It can be applied to many imaging modalities and all body parts and seek to focus on skeptical structures. In the 1980s, the concept of automated computer diagnosis was started [20], but these early attempts were not successful. Thus, it became extremely difficult to carry out a computer based analysis in medical images. Therefore, it was not easy to anticipate whether the development of CAD schemes would be successful or failure. From 2000s, there is a gradual increase in research related to CAD diagnosis of breast cancer, lung cancer, colon cancer, prostate cancer, bone metastases, coronary artery disease and congenital heart defect. Today's CAD can provide specificity up to 90 to 100% depending on the application. It may not provide accurate results every time, but can be helpful in providing preliminary diagnosis, in addition to doctors decision which is always important for final consideration. Since ultrasound has many advantages and more frequently used imaging model, we performed CAD on ultrasound images. However the interpretation of ultrasound images of any organ by computer is difficult because of large speckle noise and gray scale image. Eliminating these problems, CAD can be used as a preliminary diagnosis to assist the doctor in ultrasound scanning.

In past, [21] proposed a computer aided decision support system for kidney abnormality detection using first and second order statistical features. Automatic abnormality detection on FPGA is proposed in [22], in this approach, the textural features are extracted from manually segmented kidney, features which has more intervariance between normal and abnormal images are selected for classification. Segmenting the kidney from ultrasound images is crucial in computer aided diagnosis of kidney. Many ideas are proposed in the literature to segment kidney from ultrasound images [23]. Ultrasound kidney segmentation based on textural and shape priors is proposed in [24]. [25] proposed an algorithm to segment kidney from ultrasound images using textural based classification, considerable care should be taken to smooth the kidney boundary to reduce local fluctuations which is an overhead and also this method is based on gradient information which may not be significant always. Automatic kidney detection using Markov random fields and active contours is proposed in [26], but a manual adjustment is required before processing the image. [27] is based on image appearance and shape variations, aligning of image is necessary which is not feasible when real time detection is considered, [28] is based on machine learning techniques, but requires manual intervention to mark the points on kidney before segmentation. The method we adopted for detecting kidney in an ultrasound images is based on Viola Jones detector [29].

1.2 Evaluation

To validate the back end algorithms front end data requried. RF data for backend system analysis was obtained from [30]. Following describes RF data: Ramp and hold stress stimulus were used to initiate a creep-recovery method for imaging breast lesions. Linear transducer array from Antares

System is manually pressed into the skin surface in anterior-posterior direction for a time period of 12 sec. Compressive force is applied for the frst second and later released for remaining time. Benign patient data downloaded is biopsy-verifed and is presented with non-palpable tumours which was detected by mammography [30]. The patient was diagnosed with fibroadenoma. The algorithms developed were first tested on Matlab simulink. Later verilog code for above mentioned algorithms were developed and ported onto Kinetx 7 board. The results obtained are compared with matlab results to validate the algorithms performance.

Experiments for CAD were performed on Zed board that uses Xilinx Zynq 7000 all programmable SOC running with Xillinux operating sytems at 667 MHz clock frequency. Zedboard is a combination of FPGA and ARM Cortex-A9 [31]. The Zedboard has the computational capability to implement ultrasound signal processing algorithms. These features of the board make it ideal for rapid prototyping and proof of concept development.

Chapter 2

FPGA Based Ultrasound Backend System with Image Enhancement Technique

2.1 B-Mode system

2.1.1 Acquisition System

All ultrasound systems typically consists of four main components as shown in Fig. 2.1. The first being the transducer to transmit and receive ultrasound pulses, the second is the beam forming to condition the signal being transmitted and received. The third part consists of signal processing techniques to process the received data with high dynamic range and finally displaying the ultrasound image.

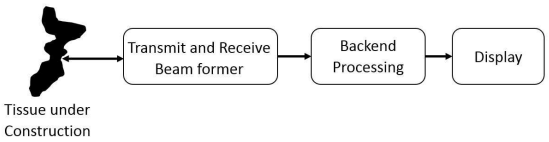

Figure 2.1: Block diagram of ultrasound image acquisition system

2.1.2 B-Mode Image Processing

The RF scan-line data received are successively placed side by side resulting in the final B-Mode image. In simpler terms, it is a signal that contains the variation in the amplitude of the RF data. The RF data has its amplitude and phase similar to that of a sinusoidal. The received RF echo data by themselves carry little information about the structure of tissue being imaged. The amplitude of the sinusoidal gives the information of the reflection and back scattering at a particular depth in the tissue. Therefore the amplitude demodulation is carried out to remove the alternations, by

quadrature demodulation and decimation using in-phase (I) and quadrature (Q) samples as shown in Fig. 2.2. The envelope of the demodulated signal having high dynamic range is detected from the RF data and should be compressed to match the dynamic range of human eye.

Figure 2.2: Basic Backend processing

After log compression, scan conversion is done, which include coordinate transformation from polar to Cartesian for curvilinear and phased array probe to reduce the artifacts while displaying and also provide user interface to zoom, rotate, etc. Scan conversion includes linear interpolation and address transformation between neighbouring pixel values to smoothen the effects of co-ordinate re-sampling as discussed in [32], [33], thus avoiding unnecessary artifacts and providing better interface to user.

2.2 Ultrasound Backend System Architecture

After receiving the processed data from beamformer which includes delay and summation of echo signals, we started our processing with envelope detection where information of the tissue is deduced by taking the absolute value of real and quadrature components [34].

Envelope Detection

Traditional approach to generate I/Q data include analog/digital base band demodulation which requires significant extra circuitry on each channel. Hence Hilbert Transform is used to reduce the amount of hardware required and get accurate values of the quadrature components as it provides 90-degree phase shift at all frequencies [35]. The Hilbert transform shifts the phase of a signal by 90 degrees i.e. positive frequency components are shifted by +90 degrees, and negative frequency components are shifted by - 90 degrees. Digital FIR filter approximations are used to implement the Hilbert transformation. FIR filter for Linear Time Invariant (LTI) systems described as follows [34]

$$\begin{aligned} y[n] &= b_0 x[n] + b_1 x[n-1] + ... + b_M x[n-M] \\ &= \textstyle\sum_{i=0}^{M} b_i x[n-i] \end{aligned}$$

where x is the input signal, y is the output signal and the constants b_i, $i = 0, 1, 2, ..., M$, are the coefficients. The Hilbert transformed data of the received echo signal can be generated by the above designed FIR Hilbert filter. The impulse response of the Hilbert filter with length N is defined as [36]:

$$h[n] = \begin{cases} \frac{2}{\pi} \frac{sin^2(\pi(n-\alpha)/2)}{n-\alpha} & n \neq \alpha \\ 0 & n = \alpha \end{cases}$$

$\alpha = (N-1)/2$. Filter order for FIR Hilbert filter is selected based on normalized root mean square error (RMSE) between ideal Hilbert filter and designed n-tap FIR Hilbert filter. Table 1 gives the comparison between various FIR Hilbert filters [37].

Table 2.1: Normalized RMSE for FIR Hilbert filters

FIR Hilbert filter order	Normalized RMSE value
16	0.0109
20	0.0096
24	0.0092
28	0.0091
32	0.0090

Dynamic Range Compression

The actual dynamic range of the received signal is around 80dB or higher depending on the ADC bits of amplifier. Amplifiers are used in the front end of ultrasound systems to transform received echo signals to digital values that are used for further processing. As the maximum dynamic range of the human eye is in the order of 30 dB [43], log transformation is used to compress the pixel values having dynamic range of 80dB to desired range [39]. Hence the signal is log compressed to 8 bits to fit the dynamic range for display.

Reconstruction and Image Enhancement

The data obtained after dynamic range compression is in Cartesian coordinates since it is assumed that linear probes are used. Thus, the received echoes are directly interpolated based on their neighbouring pixel values, generally 4 nearest neighbours. Superior image quality can be obtained by using linear interpolation with the original data that are sampled to match inter pixel spacing [40]. Point operations are applied on the image formed after interpolation to enhance the image clarity, where a function f operates on single pixel in image I to obtain a full scale contrast stretch image J . It is given by

$$J(i,j) = f[I(i,j)]; 0 \leq i \leq N-1, 0 \leq j \leq M-1$$

where M, N are the dimensions of the image I. Point operations provide a flat histogram as it makes rich use of available gray scale and give lots of texture over many gray levels.

2.3 FPGA based Backend System Implementation and Results

Hardware software co-simulation was done to study the performance of the proposed ultrasound backend system. Computationally intensive modules such as envelope detection, log compression

and scan conversion are specifically implemented on Kintex 7 FPGA platform (Fig. 2.3) [41] as shown in to assure that the desired output is produced.

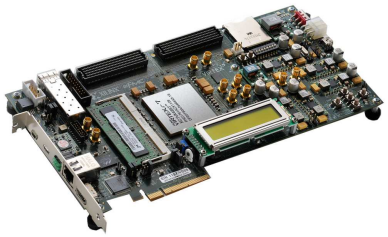

Figure 2.3: Kintex 7 FPGA

The system is implemented in the hardware description language (VHDL) and synthesized with Kintex-7 FPGA, using Xilinx system generator (Xilinx, Inc.) and MATLAB Simulink (Mathworks, Inc.). RF data for backend system analysis were obtained from [30]. Following describes RF data: Ramp and hold stress stimulus were used to initiate a creep-recovery method for imaging breast lesions. Linear transducer array from Antares System is manually pressed into the skin surface in anterior-posterior direction for a time period of 12 sec. Compressive force is applied for the first second and later released for remaining time. Benign patient data downloaded is biopsy-verified and is presented with non-palpable tumours which was detected by mammography [30]. The patient was diagnosed with fibroadenoma. 360 scan lines of RF data were obtained from transducer and stored in MATLAB workspace. Fig. 2.4 shows plot of one scan line having 1600 samples, that are converted from floating point to fixed point numeric precision to control cost and consume less power.

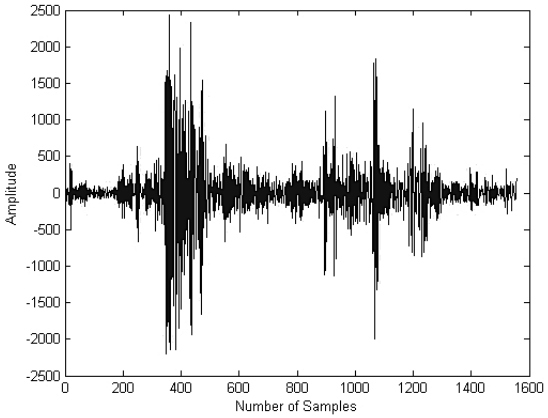

Figure 2.4: RF scan line

With reference to Table 2.1 32-tap filter provides least RMSE (0.0090), hence we implemented 32-tap FIR Hilbert filter having the magnitude response shown in Fig. 2.5 to obtain in-phase and quadrature phase components.

Fig. 2.6 shows block diagram of envelope detection, onto which normalized RF scan line is passed.

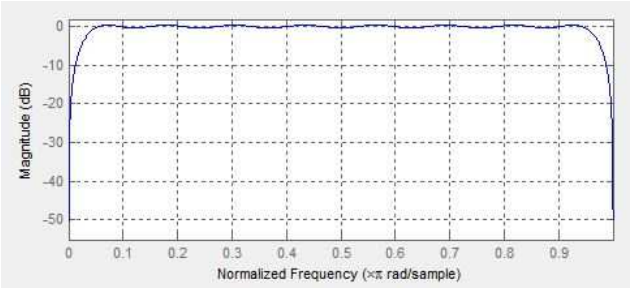

Figure 2.5: Frequency response of 32-tap FIR Hilbert filter

The quadrature components obtained from Hilbert filter block are passed through envelope detector to detect the envelope of the RF signal. Fig. 2.8b shows the envelope of input signal shown in Fig. 2.4

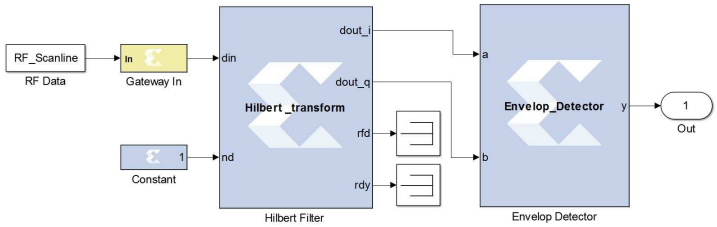

Figure 2.6: Envlope detection block

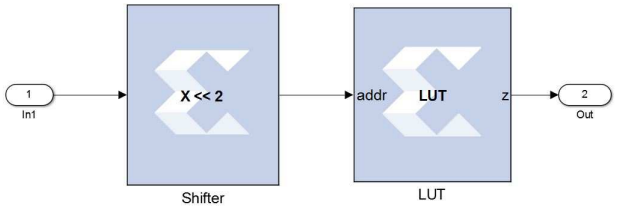

Figure 2.7: Compression block

Fig. 2.7 shows the block diagram of log compression technique using 16-KB look up table (LUT) to obtain the compressed data. Fig. 2.8a shows the log compressed data having less dynamic range compared to original data as in Fig. 2.8b. Fig. 2.9a and Fig. 2.9b show images with and without log compression.

For the image construction, we mapped the log compressed data to their respective gray levels and displayed the final image as in Fig. 2.9b. Later we applied our image enhancement technique which flattens the histogram and enhances the contrast of image, making it better than the traditional image developed on ultrasound machines. Fig. 2.9c shows the enhanced final image that was obtained.

Table.2.2 gives the utilization summary for the whole implementation, the used devices, available in the port, and the utilization percentage using Kintex-7 FPGA.

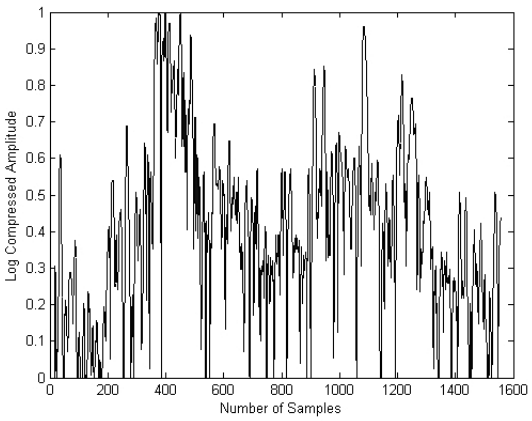

(a) Log compressed data

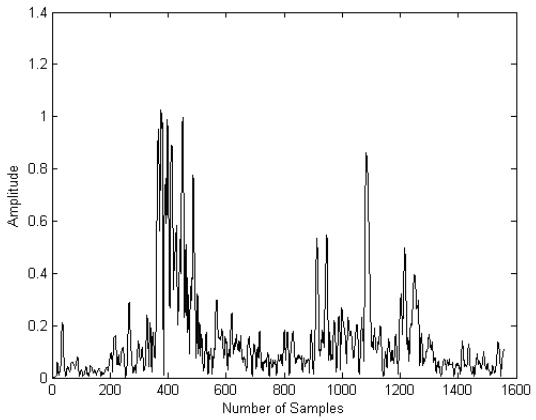

(b) Envelope detected data

Figure 2.8: Waveforms at various levels

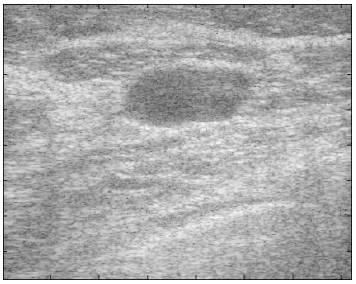

(a) Image without compression

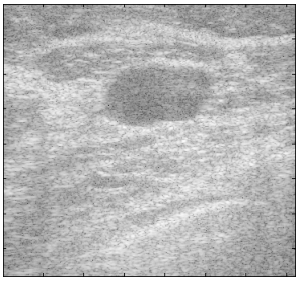

(b) Image after compression

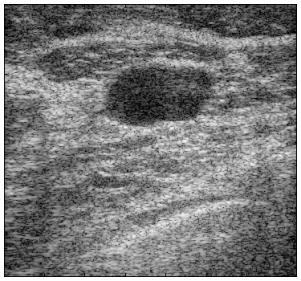

(c) Final image after enhancement

Figure 2.9: Ovearall image anlaysis

Table 2.2: Device utilization summary

Slice Logic Utilization	Used	Available	Utilization
Number of Slice Registers	1,902	407,600	1%
Number used as Flip Flops	1,902	-	-
Number of Slice LUTs	2,526	203,800	1%
Number used as logic	2,224	203,800	1%
Number using O6 output only	2,072	-	-
Number using O5 output only	8	-	-
Number using O5 and O6	144	-	-
Number used as Memory	296	64,000	1%
Number used as Shift Register	296	-	-
Number using O6 output only	296	-	-
Number used exclusively as route-thrus	6	-	-
Number with same-slice register load	6	-	-
Number of occupied Slices	798	50,950	1%
Number of LUT Flip Flop pairs used	2,611	-	-
Number with an unused Flip Flop	739	2,611	28%
Number with an unused LUT	85	2,611	3%
Number of fully used LUT-FF pairs	1,787	2,611	68%
Number of unique control sets	6	-	-
Number of Slice registers lost to control set restrictions	18	407,600	1%
Number of bonded IOBs	111	500	22%
Average Fanout of Non-Clock Nets	3.25	-	-

2.4 Conclusion

Wee were able to present the FPGA based ultrasound backend system that would process the echo signals received from tissues. While processing we were able to develop envelope detection block using 32-tap FIR Hilbert transform, log compression block to compress the dynamic range, interpolation to reduce the blocking artifacts and finally image quality is enhanced using full scale contrast stretch to give a better contrast than traditional ultrasound systems. Implementation on FPGA reduces the cost of development and also provides a platform for the researchers to develop new algorithms and implement them which can lead to a new era of ultrasound imaging.

Chapter 3

Compression Techniques For Ultrasound Imaging System

3.1 Ultrasound Signal Model

The returned echo signals form the tissue are random as the scatterers location considered are random [42]. The received echo, $e(t)$, is denoted by

$$e(t) = \sum_{n=1}^{N} \alpha_i cos(\omega_0 t + \phi_i) \tag{3.1}$$

where ω_0 is center frequency of RF signal and N is the scatterer number. α_i and ϕ_i denote to amplitude and phase of the i^{th} scatterer respectively. For large values of N the echo can be expressed as

$$e(t) = Acos(\omega_0 t) - Bsin(\omega_0 t) \tag{3.2}$$

According to central limit theorem, A and B are identical gaussian random variables with zero mean and are given by

$$A = \sum_{n=1}^{N} \alpha_n cos(\phi_n); B = \sum_{n=1}^{N} \alpha_n sin(\phi_n) \tag{3.3}$$

The envelope R of the received RF echo, is given by

$$R = \sqrt{A^2 + B^2} \tag{3.4}$$

The probability density function $f(r)$ of the envelope can be modelled as Nakagami and is given by [58]

$$f(r) = \frac{2m^m r^{2m-1}}{\Gamma(m)\Omega^m} exp(-\frac{m}{\Omega} r^2) U(r) \tag{3.5}$$

where Ω is a scaling parameter and m is the Nakagami parameter that is evaluated from mean and variance of envelope, given by

$$m = \frac{[E(R^2)]^2}{E[R^2 - E(R^2)]^2} \tag{3.6}$$

where $E(.)$ gives the expectation, scaling factor Ω is given by

$$\Omega = E(R^2) \tag{3.7}$$

The cumulative distribution function $F(r)$ is given by

$$F(r) = \int_0^r \frac{2m^m y^{2m-1}}{\Gamma(m)\Omega^m} exp(-\frac{m}{\Omega}y^2)dy = P(\frac{m}{\Omega}r^2, m) \tag{3.8}$$

where $P(...)$ is the incomplete Gamma function. The density function obtained varies according to values of m. For $m = 0.5$, half Gaussian is obtained, $m = 1$ we get Rayleigh and for values $m > 1$ we get Rician distribution.

3.2 Envelope Compression in B-Scan Imaging

The dynamic range of the received RF data envelope in ultrasound imaging is very large as it depends on the TGC amplifier, ADC bits used in the front end, and depth of tissue being measured. As the maximum dynamic range of ultrasound signal has 12 bits, handheld ultrasound system cannot have display that can support such high dynamic range. Hence compression technique is necessary to compress dynamic range to usually 7 or 8 bits that suits well for human eye having dynamic range in the order of 30dB [43]. Ultrasound systems achieves this range compression using non-linear compression technique that selectively compresses large input signals.

3.2.1 Logarithmic Compression

High dynamic range of an image can be compressed by replacing each of the input value by its logarithmic value, hence low intensity values are enhanced and high intensity values are compressed providing the required dynamic range. The transfer function for logarithmic compression is [44]

$$X = DlnA + L \tag{3.9}$$

Where D is the dynamic range compression parameter, A is the value of received echo signal, L is the linear gain factor and X is the compressed output signal.

Let A_{min} and A_{max} be the minimum and maximum input values of the signal whose corresponding output values are X_{min} and X_{max} by the above compression technique, then difference of the output is

$$X_{max} - X_{min} = Dln(\frac{A_{max}}{A_{min}}) \tag{3.10}$$

Since L can be considered as constant, has no effect on output signal characteristics [45]. The input

dynamic range R is given by

$$R = 20ln(\frac{A_{max}}{A_{min}}) \tag{3.11}$$

Hence the output dynamic range and input dynamic range can be equated as

$$D = \frac{20}{R}(X_{max} - X_{min}) \tag{3.12}$$

3.2.2 Gamma Compression

Gamma compression is a non-linear operation that is used to compress the dynamic range. Gamma correction according to power law expression is defined as

$$X = GA^{\gamma} \tag{3.13}$$

where G is a constant, X and A are the output and input values respectively. Gamma value, $\gamma > 1$ is called gamma compression and gamma value, $\gamma < 1$ is called gamma expansion. Gamma compression highlights information in dark regions, saturating bright regions towards white and gamma expansion highlights details in bright region diminishing details in dark region. Image is divided into regions of bright and dark to determine the gamma coefficients [46]. Mean of each region is given by

$$M_d = \sum X/N_d, if(X \leq x_m) \tag{3.14}$$

$$M_b = \sum X/N_b, if(X \geq x_m) \tag{3.15}$$

where X is the input signal, x_m is the user defined point for dividing the regions. M_d and M_b are the means of dark and bright regions. N_d and N_b are the number of samples in each region. Considering these parameters the gamma coefficients for compression and expansion respectively are

$$\gamma_c = \alpha sin\left(\frac{(x_m - M_d)\pi}{2x_m}\right) + 1 \tag{3.16}$$

$$\frac{1}{\gamma} = \alpha sin\left(\frac{(M_b - x_m)\pi}{2(255 - x_m)}\right) + 1 \tag{3.17}$$

where α depends on the dynamic ranges of display devices. α value is high for displays with low dynamic range and is low for displays having high dynamic range.

3.2.3 Wavelet based Compression

Filter Banks

The two techniques discussed earlier are global tone mapping methods that use compressive functions such as a power function to map input and output signals. More localized techniques are needed to compress the dynamic range initially and later enhance if necessary [47]. The block diagram of this compression technique is shown in Fig. 3.1

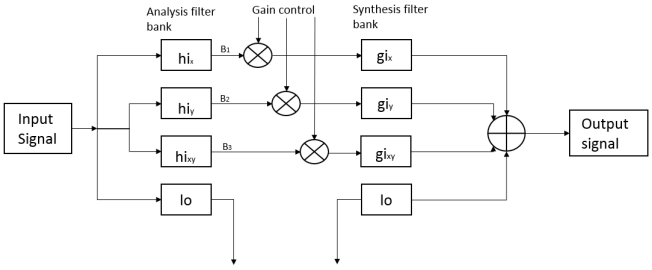

Figure 3.1: Block diagram of dynamic range Compressor

This technique is based on analysis-synthesis filter bank, where $hi_x, hi_y, ...$ are called analysis filter banks to split the signals to subband signals $B_1, B_2, ...$ respectively and $gi_x, gi_y, ...$ are called the synthesis filter banks whose output when summed together reconstructs back the original signal. The filter taps of analysis filter bank are spread and padded with zeros, high pass filter f_1 increases from $[1, -1]$ initially to $[1, 0, -1]$ and later $[1, 0, 0, 0, -1]$ on succeeding stages, similarly low pass filter $f_0 = [1, 1]$ is padded with zeros, resulting in $2D$ zero padded filters $(hi_x, hi_y, hi_{xy}, lo)$ when f_0 and f_1 are combined in both x and y directions separately. The synthesis filters are obtained by temporally reversing f_1 and combining with f_0.

Gain Control

The gain control depends on the activity map which varies from point to point, hence gain map is formed depending on the subband image. Gain map can be computed by using aggregated activity map (A_{ag}) by pooling activity maps (A_i) over scales and orientations:

$$A_{ag} = \sum_{i=1,...3n+1} A_i \tag{3.18}$$

Single gain map $G_{ag} = p(A_{ag})$, where $p(.)$ is a non-linear function given by

$$p(A_i) = \left(\frac{A_i + \varepsilon}{\delta} \right)^{\gamma - 1} \tag{3.19}$$

where γ is a compressive factor between 0 and 1, ε is a noise level related parameter, δ is gain control stability level set to one tenth the average of A_{ag}.

3.3 Results

RF scan lines data for analysis were obtained from [48]. Following describes RF ultrasound data used for the performance analysis of the various compression techniques: Fig. 3.2 indicates the scan line data recorded by University of Illinois, patient having benign tumor is tested using ramp and hold stress to measure the lesions in breast using creep-recovery method. A linear transducer was used to scan nearer the front and behind the tissue for around 15 seconds. Benign patient data

downloaded had tumor that is recognized using palpation and was verified by biopsy. The patient was diagnosed with fibroadenoma.

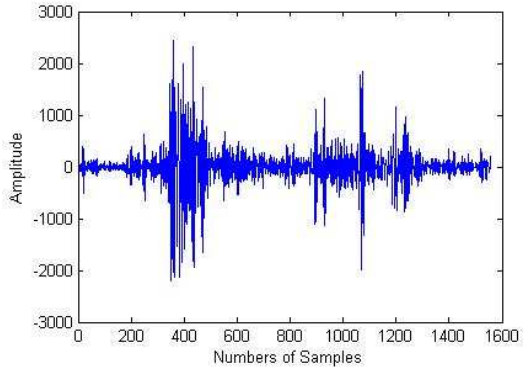

Figure 3.2: Received Echo data

Log-compressed, Gamma compressed and Wavelet based compressed images as shown in Fig. 3.3b, Fig. 3.3c, and Fig. 3.3d respectively are compared with image that is not compressed as shown in Fig. 3.3a. The compression techniques are assessed based on various visual quality assessment indices, that include Multi-scale SSIM index (MSSIM), Structural SIMilarity (SSIM) index, Pixel based Visual Information Fidelity (VIFP) and Peak Signal-to-noise-ratio (PSNR).

SSIM and MSSIM are methods that can be used to measure the similarity between images [49] and [50]. The SSIM index measures the image quality based on an initial uncompressed image as reference with the other images. SSIM is designed to improve on traditional methods like mean squared error (MSE) and peak signal-to-noise ratio (PSNR). SSIM index between I and J at a point (i, j) is expressed as

$$SSIM_{I,J}(i,j) = LL_{I,J}(i,j)LC_{I,J}(i,j)LS_{I,J}(i,j) \tag{3.20}$$

where $LL_{I,J}(i,j)$ is a measure of Local Luminance similarity, $LC_{I,J}(i,j)$ is a measure of Local Contrast similarity, $LS_{I,J}(i,j)$ is a measure of Local Structure similarity.

MS-SIM values are obtained by calculating values of cross-correlation and variance of image at various scales obtained by low pass filtering and sub sampling, by factor of 2 in spatial directions x and y [51]. It is given by:

$$MS - SIM(X,Y) = m_k(X,Y)^{\alpha_k} \prod_{k=1}^{K} v_k(X,Y)^{\beta_k} r_k(X,Y)^{\gamma_k} \tag{3.21}$$

where $m_k(X,Y)$, $v_k(X,Y)$, and $r_k(X,Y)$ respectively correspond to the mean, variance, and cross-correlation component computed from scale k.

The Visual Information Fidelity (VIF) measure for assessment of image quality based on mutual information between reference image and distorted image [52]. Mutual information between input and output of Human Visual System (HVS) channel of reference image is then compared to HVS

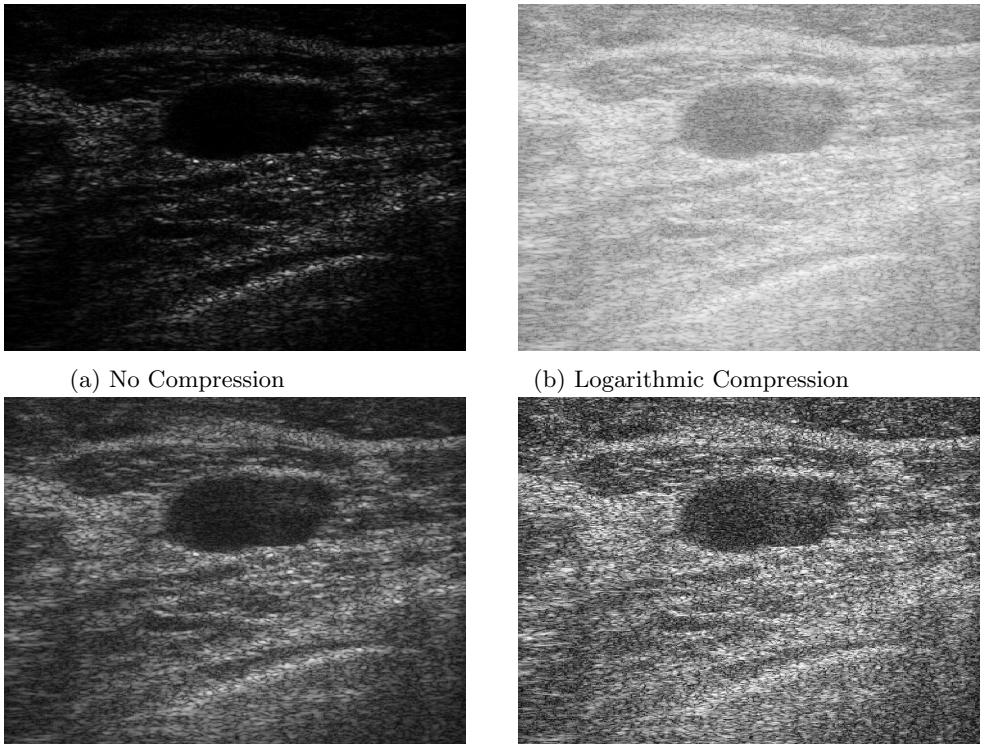

(a) No Compression (b) Logarithmic Compression

(c) Gamma Compression (d) Wavelet based Compression

Figure 3.3: US image whith various compression techniques

channel for compressed image.

$$VIF = \frac{\sum I(C^{N,j}; F^{N,j}|s^{N,j})}{\sum I(C^{N,j}; E^{N,j}|s^{N,j})} \tag{3.22}$$

where $I(C^{N,j}; F^{N,j}|s^{N,j})$ and $I(C^{N,j}; E^{N,j}|s^{N,j})$ are mutual information of reference and compressed images respectively.

Mean Square Error and Peak Signal to Noise Ratio are calculated using the following equations:

$$MSE = E_i(I_i - J_i)^2 \tag{3.23}$$

where E_i is the expectation, I_i is the reference image pixel value and J_i is query image pixel value.

$$PSNR = 10log_{10}(255^2/MSE) \tag{3.24}$$

Table 3.1 gives various indices of compressed images of 8 bit size with reference to uncompressed image of 12 bit size. From the table it is clearly observed that gamma compressed image has a good match with the original uncompressed image when compared to other compression techniques like log compression and wavelet compression technique.

	MSSIM	SSIM	VIFP	PSNR
Log Compressed Image	0.2520	0.0093	0.9323	3.4875
Gamma Compressed Image	0.2727	0.0130	0.9740	9.9145
Wavelet based compression	0.0966	0.0030	0.9477	6.1237

Table 3.1: Comparisons with uncompressed image and various compressed images

3.4 Conclusion

Various Compression techniques were assessed based on SSIM index. Gamma compression gave best results when compared to original image, this information might be helpful for clinicians for in depth diagnosis. Gamma compression is implemented using Look Up Table (LUT) approach, hence ensures minimum hardware complexity.

Chapter 4

Preliminary CAD On Ultrasound Imaging Device

Fig. 4.1 shows the FPGA based CAD implementation of the classifier to determine the abnormality of organ [22] in ultrasound images. In this work, we implemented preliminary CAD for kidney

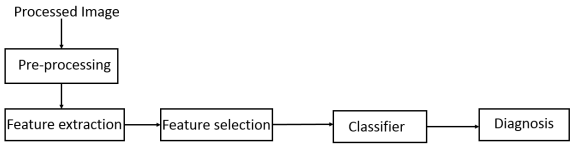

Figure 4.1: System Architecture for CAD implementation on FPGA

diagnosis. Preliminary CAD is used to classify normal and abnormal kidney images, not further classifying into abnormalities like cyst, stones, etc. Fig. 4.2 shows images of normal and abnormal kidney, abnormality in this case is due to cysts. Noise in final image leads to wrong diagnosis of

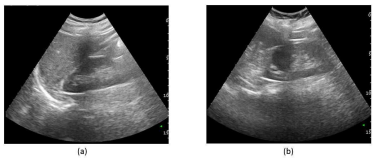

Figure 4.2: (a) Normal kidney (b) Abnormal kidney

patient, hence acquired image is processed using wavelets [53]. After noise removal, features of organ are extracted automatically by our proposed algorithm, out of the features extracted only a few are selected by feature selection algorithm, to validate any abnormality in organ at the classifier block. Based on the classifier decision, priority of sending patient data can be changed to high in case of emergency.

4.1 Pre-processing

Speckles are spatially correlated multiplicative noise [54], present at all stages of image acquisition [55]. These are granular like structures in the B-mode ultrasound images and can be denoised

using various techniques starting from sample mean and variance to various nonlinear techniques. Denoisng of these speckles in our paper is done using threshold wavelet coefficients by transforming image to wavelet domain, which makes the image sparse in nature [56]. In wavelet domain the original image coefficinets will be of large value and when noise is added to original image the value of coefficients will be small. Hence coefficients with smaller values indicating the presence of noise are set to zeros, to eliminate noise. Global threshold is applied according to which values below threshold are set to zero and the remaining values are made to start from zeros. The original image is taken and threshold is calculated using global threshold λ given by:

$$\lambda = \sqrt{2 * log(n)}$$

where n is total number of pixels in image given by N*M where N, M are the dimensions of image.

Discrete Wavelet Transform (DWT) of the image is calculated to three decomposition levels and threshold applies to these levels. Inverse Discrete Wavelet Transform (IDWT) is performed on the resultant wavelet coefficients, to obtain the denoised image. Fig. 4.4 shows both noised and

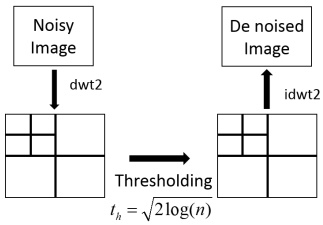

Figure 4.3: Denoising using 2 level DWT: dwt2, idwt2

denoised image, denoised image is obtained by applying DWT. Denoised images reduce errors while classifying images as normal and abnormal.

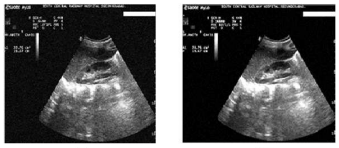

Figure 4.4: (a)Noisy image (b) Denoised image

4.2 Feature Extraction

Database of 394 images were collected of which 330 are normal and 64 are abnormal images of kidneys. Initially, manual segmentation is done on 180 images - 150 normal and 30 abnormal in the presence of a well trained doctor to extract basic features which are used to train the system that can classify kidney. These features are grouped into three classes: Adaptive features, Histogram features and Haralick features [57]. Adaptive features include location, echo texture and size. We are introducing the term adaptive features of kidney which are the features that vary from person to person and cannot be generalized. For example, longitudinal length of normal kidney varies from

8 cm for short people and 12 cm for tall people, echo texture of kidney is dark for thin people and is clearly visible but muscled people have light echo texture making it difficult to trace the shape of kidney. Comparative study between two kidneys is necessary to get the adaptive features like determining the change in size of the kidney. This method eliminates false negative of abnormality detection in case of diabetics where kidneys are usually larger in size.

After denoising, histogram and haralick features are calculated. Extracting features based on the histogram gives first order statistical features of an image, which are useful for object classification. There are 6 such histogram features which include skewness, mean, energy, variance, entropy, and kurtosis. There are 22 Haralick features which include contrast, auto correlation, correlation, cluster shade, cluster prominence, dissimilarity, maximum probability, homogeneity, sum of squares, sum average, sum variance, sum entropy, difference variance, etc. These features are extracted from co-occurrence matrix G of dimension Ng (number of gray levels) as given below, each element $P(i;j)$ gives the probability of occurrence of gray level i in the specified spatial relationship with gray level j.

$$G = \begin{pmatrix} P(1,1) & \dots & P(1,N_g) \\ \vdots & \ddots & \vdots \\ P(N_g,1) & \cdots & P(N_g,N_g) \end{pmatrix}$$

$$\mu_x = \sum_{i=1}^{N_g} iP_x(i), \qquad \mu_y = \sum_{j=1}^{N_g} jP_y(j)$$

$${\sigma^2}_x = \sum_{i=1}^{N_g} (P_x(i) - \mu_x)^2, \quad {\sigma^2}_y = \sum_{j=1}^{N_g} (P_y(j) - \mu_y)^2$$

$$P_x(i) = \sum_{i=1}^{N_g} P(i,j), \qquad P_y(j) = \sum_{j=1}^{N_g} P(i,j),$$

$$P_{x+y}(k) = \sum_{i,j=1}^{N_g} P(i,j)$$

where μ_x, μ_y, σ_x, σ_y are the mean and standard deviation of P_x and P_y. $P_x(i)$, $P_y(j)$ is sum of i^{th} row and j^{th} column respectively.

4.3 Feature Selection

Using all the 28 features obtained from feature selection for kidney abnormality detection requires lots of resources on the ultrasound machine, hence there is a need to select minimum features that are enough to distinguish between images of normal and abnormal kidneys. Hence out of all the above mentioned features extracted, only few features are selected based on Genetic Algorithm (GA) [58], an optimization technique. It maintains a population of constant size which represents a sample space to be searched as explained in Algorithm 1. Population refers to features extracted and is evaluated based on overall fitness depending on the application domain. The next generation of individuals is developed using crossover and mutation. Individuals based on crossover are formed by selecting a point from selected parent gene structure and exchanging the remaining segments. Individuals based on mutation are formed by changing one or more components of selected individual randomly. Fitness values are calculated for the new generation population and value of generation is incremented. This procedure is repeated until termination condition is met (e.g. one individual meets desired fitness

Algorithm 1 Genetic Algorithm (n, χ, μ)

Initial: generation (k) = 0;
P_k:= population of n randomly-generated individuals;
Evaluate P_k;
Comment: n is the number of individuals in the population;
χ is the fraction of the population to be replaced by crossover in each iteration;
μ is the mutation rate.

1: **do**
2: {
3: **Create generation** $k + 1$:
4: **Copy:**
5: Select $(1 - \chi)$ X n members of P_k and insert into P_{k+1};
6: **Crossover:**
7: Select χ X n members of P_k; pair them up; produce offspring; insert the offspring into P_{k+1};
8: **Mutate:**
9: Select μ X n members of P_{k+1}; invert a randomly-selected bit in each;
10: **Evaluate** P_{k+1}:
11: Compute fitness (i) for each $i \in P_k$;
12: **Increment:**
13: k := k + 1;
14: }
15: **while** fitness of fittest individual in P_k is not high enough; **return** the fittest individual from P_k;

or required generations have passed). For our application, to determine abnormality in kidney, algorithm terminated at third generation (i.e at k=3) and finally 12 features (P_k=12) are obtained as an output of GA. The efficiency of classification is defined as the proportion of actual positives correctly identified to total positives present in database. Fig. 4.5 plots the efficiency calculated for different parameter lengths. Since efficiency is constant, from parameter length 8, 9 and 10, out of 12 features obtained, only 9 features are selected for further analysis. The selected features include mean, skewness, kurtosis, cluster shade, correlation, sum average, max probability, homogeneity, sum of squares, longitudinal length of the kidney is considered as 10th feature. Longitudinal length is considered as mandatory feature as it detect true positives with least computation. If a person has pain near kidney and during diagnosis if the size of kidney is more than 12cm than it can be considered as abnormal without further analysis.

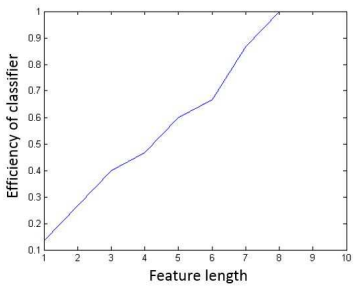

Figure 4.5: Efficiency plot for various parameter length

Finally these 10 optimized features are considered for further classification rather than considering all the features. The computation of these features are as follows:

$$Mean, \mu = \frac{1}{MN} \sum_{i,j} I(i,j) \tag{4.1}$$

$$Skewness = \frac{1}{MN} \sum_{i,j} \frac{(I(i,j) - \mu)^3}{\sigma^3} \tag{4.2}$$

$$Kurtosis = \frac{1}{MN} \sum_{i,j} \frac{(I(i,j) - \mu)^4}{\sigma^4} \tag{4.3}$$

$$sum\ avg = \sum_{i=1}^{2N_g} iP_{x+y}(i) \tag{4.4}$$

$$correlation = \sum_{i,j=1}^{N_g} \frac{\{i \times j\} \times P(i,j) - \{\mu_x \times \mu_y\}}{\sigma_x \sigma_y} \tag{4.5}$$

$$cluster\ shade = \sum_{i,j} (i + j - \mu_x - \mu_y)^3 P(i,j) \tag{4.6}$$

$$homogeneity = \sum_{i,j} \frac{P(i,j)}{1 + |i - j|} \tag{4.7}$$

$$max\ prob. = \sum_{i,j=1}^{N_g} \max(P(i,j)) \tag{4.8}$$

$$sum\ of\ squares = \sum_{i,j} (i - \mu_x)^2 P(i,j) \tag{4.9}$$

where $I(i,j)$ is the intensity value at i^{th} row and j^{th} column. For further details on these feature calculation, refer to [59].

Sl.No	Feature	Desired Range
1	Length	8-12 cm
2	Sum Average	0.414-4.182
3	Mean	1.08-1.336
4	Skewness	2.822-7.708
5	Kurtosis	11.06-71.152
6	Correlation	0.971-0.987
7	Cluster Shade	72-243
8	Homogeneity	0.993-0.998
9	Maximum Probability	0.840-0.969
10	Sum of Squares	0.828-10.756

Table 4.1: Desired range of features extracted from normal kidney

4.4 Classifier

The classifier is initially trained with features having a desired range as mentioned in Table 4.1. The table we obtained is with reference to previous tables given in [57] which have less features and

no range. We thus tabulated more features with a range for normal kidney images. In the Table 4.1 length is an adaptive feature and has to be trained every time depending on the patient, for example, in the case of diabetics the size of the kidney will be more than 12 cm but this case is to be identified as normal. Intensity and Haralick features need not be changed as they are fixed. Steps involved in the CAD analysis are shown in Algorithm 2.

Algorithm 2 Automatic Kidney Classification

Initial: Set *Threshold* values
Set *abnormal_count*=0 ;

procedure DECISION MAKER(*Extracted Features*)
    Comment: Calculate mean, skewness, krutosis, correlation, cluster shade, homogeneity, maximum probability, sum of squares, sum average intervals.
    Calculate *length of normal kidney*;
    Set length.threshold = length of normal kidney;
    Calculate *Data.length_interval*;
    if *Data.length* $\neq$ *length.threshold* **then**
            Decide the kidney is abnormal;
            Send data with high priority;
        Calculate *Data.mean_interval*;
        Calculate *Data.skewness_interval*;
        Calculate *Data.krutosis_interval*;
        Calculate *Data.correlation_interval*;
        Calculate *Data.clustershade_interval*;
        Calculate *Data.homogeneity_interval*;
        Calculate *Data.maximumprobability_interval*;
        Calculate *Data.sumofsquares_interval*;
        Calculate *Data.sumaverage_interval*;
        if *Data exceeds Threshold* **then**
            Transmit the data immediately;
            Set *abnormal_count*=1;
        else
            Set *length.threshold* parameter;
            abnormal_count = 0;
        end if
    else
        Decide the patient is normal;
        Transmit the data;
    end if
end procedure

Depending on the patient's condition, the longitudinal length of normal kidney is considered as a threshold. Later 10 features extracted from a feature selection block which includes the length of the kidney are fed as inputs to classifier block. The intervals are then compared with threshold values and if any feature exceeds the threshold limit, then the classifier decides that the kidney is abnormal and sends the data to cloud with high priority requesting doctor for immediate diagnosis. If all the features are in the normal range, then data is sent to the cloud, without any priority, doctors can go through reports whenever possible.

The proposed CAD algorithm is ported on FPGA for validation, true positives and true negatives are calculated on a database of 394 images. As mentioned above, parameter length of 10 is considered

to validate the algorithm 2, it indicates normal or abnormal with text N or A respectively. This text is included on display image as shown in Fig. 4.6 and Fig. 4.7.

Figure 4.6: Normal case being detected on FPGA

Figure 4.7: Abnormal case being detected on FPGA

4.5 Hardware Complexity Analysis of proposed CAD algorithm

Hardware complexity of our algorithm for abnormality detection is calculated in terms of gates and transistors [60],[61]. Complexity of each feature extraction and classification are calculated as follows.

4.5.1 Complexity analysis for feature extraction

Table 4.1 shows the selected features for feature extraction. Fig. 4.8a to Fig. 4.11 shows the hardware architecture of selected features. Input to the system for calculating mean, skewness, kurtosis is image pixel values and for cluster shade, correlation, maximum probability, sum of average, sum of square, homogeneity is gray level co-occurrence matrix values.

Fig. 4.8a shows hardware architecture to determine mean. It requires 16 bit adder to add pixel values based on element index and 16 bit shifter to divide result of adder by total number of pixels. Fig. 4.8b shows hardware architecture to determine variance. It requires 16 bit adder to add total pixels, 16 bit subtractor for subtracting values of mean from pixel values, Multiplier for squaring the result obtained and 16 bit shifter to divide the final value by total number of pixels. Fig. 4.8c shows hardware architecture to determine skewness. It requires 16 bit adder to add total pixel values, 16 bit subtractor for subtracting values of mean from pixel values, two multipliers to compute cube of the result obtained and finally 16 bit shifter for dividing the result by constant. Constant in this case is the product of total number of pixels in image and σ^3 which is product of variance and standard deviation.

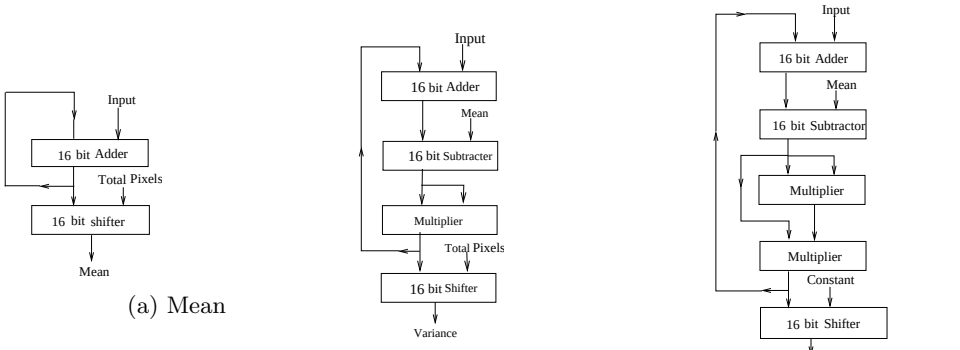

(a) Mean (b) Variance (c) Skewness

Figure 4.8: Hardware architecture of a) Mean b) Variance c) Skewness

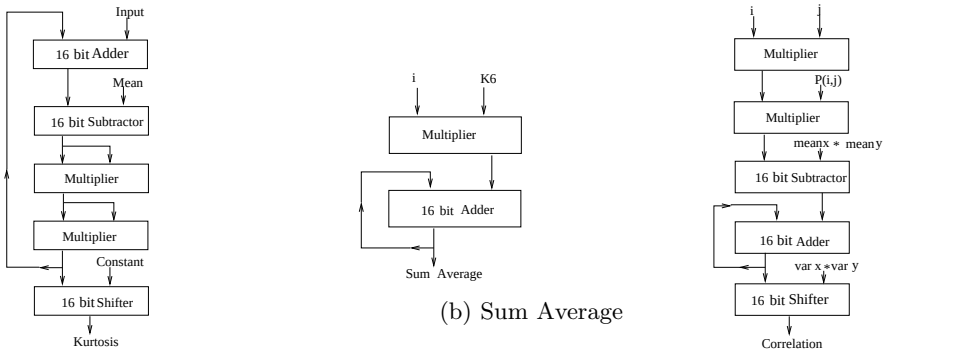

(a) Kurtosis (b) Sum Average (c) Correlation

Figure 4.9: Hardware architecture of a) Kurtosis b) Sum Average c) Correlation

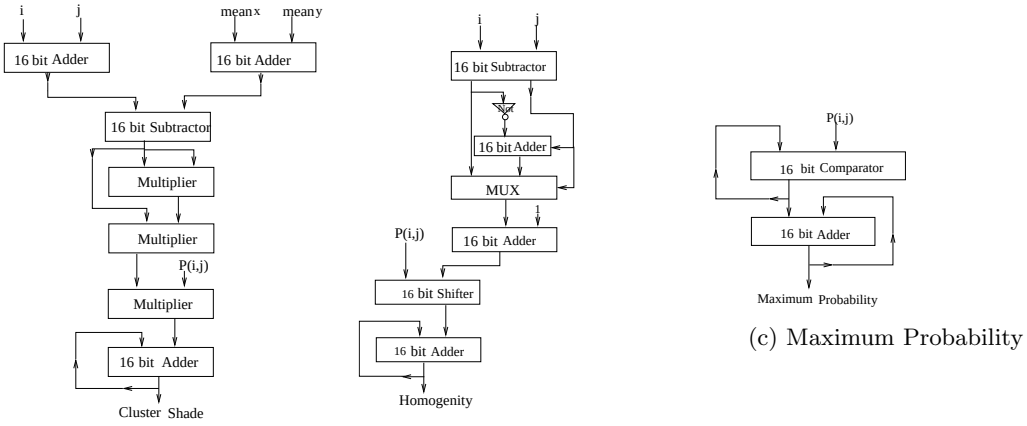

(a) Cluster Shade (b) Homogenity (c) Maximum Probability

Figure 4.10: Hardware architecture of a) Cluster Shade b) Homogenity c) Maximum Probabilityn

Fig. 4.9a shows hardware architecture to determine Kurtosis. It requires 16 bit adder to add total pixel values, 16 bit subtractor for subtracting values of mean from pixel values, two multipliers to compute 4^{th} power of the result obtained and finally 16 bit shifter for dividing by constant which is product of $variance^2$ and total number of pixels in image. Fig. 4.9b shows hardware architecture to determine sum average. It requires multiplier to find product of constant $K6$ defined as mutual probability obtained from GLCM features and index of image, both inputs are given to multiplier and later 16 bit adder is used to add the values obtained from multiplier. Fig. 4.9c shows hardware architecture to determine correlation. It requires two multipliers one to multiply indices of image and result is later multiplied with elements in GLCM matrix at other multiplier. The result obtained is subtracted from product of *mean x* and *mean y*, which are mean along x and y axis using 16 bit subtractor. One 16 bit adder is used to add value obtained along all the indices and later divided by product of *var x* and *var y* which are variance along x and y axis respectively.

Fig. 4.10a shows hardware architecture to determine cluster shade. It requires two 16 bit adders, one to add sum of indices and other to add mean values along x and y axis. The result of these adders is given to 16 bit subtractor. Cube of the result is obtained from two multipliers, other multiplier is used to take the product of result and probability value at that particular index obtained using GLCM matrix. Finally 16 bit adder is used to sum the values from each element. Fig. 4.10b shows hardware architecture to determine homogenity. It requires one 16 bit subtractor to find the difference between index of pixel values, one Not gate, one 16 bit adder and one MUX to ensure result of subtractor is always positive. One 16 bit adder is used to add constant one to the result obtained from MUX. The obtained value divides probability value of each element obtained from GLCM matrix with result obtained from adder using 16 bit shifter and later 16 bit adder is used to sum the results from every element. Fig. 4.10c shows hardware architecture to determine maximum probability. It requires 16 bit comparator to find maximum probability and 16 bit adder to sum of maximum probability of each element in the GLCM matrix.

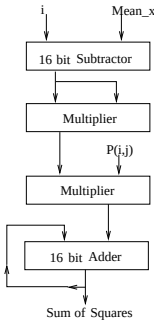

Figure 4.11: Hardware architecture of Sum Of Squares

Fig. 4.11 shows hardware architecture to determine sum of squares. It requires 16 bit subtractor to find difference between element index along x axis and mean along x axis. Square of result is obtained using multiplier and result is multiplied with probability obtained from GLCM matrix using other multiplier. Finally 16 bit adder is used to find the sum of every element and get the final result.

Table 4.2: Hardware complexity of arithmetic blocks in terms of logic gates

	NAND	AND	OR	NOR	XOR	NOT
16 Bit Adder	32	8	4	-	16	-
16 Bit Subtractor	-	31	15	-	48	-
16 Bit Multiplier	160	40	8	-	-	16
16 Bit Shifter	-	-	-	-	96	-
Comparator	-	64	16	16	-	32
MUX	4	-	-	-	-	-

Table 4.2 shows the hardware complexity of arithmetic blocks in terms of logic gates.

Table 4.3: Hardware complexity of features calculation in terms of logic gates

Features	NAND	AND	OR	NOR	XOR	NOT
Mean	32	8	4	-	112	-
Variance	192	79	27	-	160	16
Skewness	352	119	35	-	160	32
Kurtosis	352	119	35	-	160	32
ClusterShade	576	175	51	-	96	48
Sum of Average	192	48	12	-	16	16
Sum of Square	352	119	35	-	64	32
Homogeneity	100	56	27	-	192	1
Correlation	352	119	35	-	160	32
Max Prob	32	72	20	16	16	32
Total Gates	2532	914	281	16	1136	241

Table 4.4: Hardware complexity in terms of CMOS Transistors

Type of logic gate	No. of gates used	No. of CMOS Transistors
NAND	2532	10128
AND	914	5484
OR	281	1686
XOR	16	96
NOR	1136	4544
NOT	241	482

From Table 4.3 we could calculate number of logic gates required to compute the hardware complexity in terms of logic gates. Hence a total of 5120 gates are required to compute the features from kidney images. Table 4.4 gives total number of Complementary Metal Oxide Semiconductor (CMOS) transistors required to implement the feature extraction which are 22,420 in this case.

4.5.2 Complexity analysis for classifier

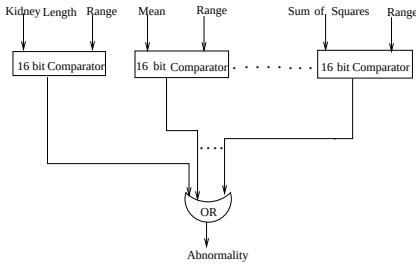

Figure 4.12: Hardware architecture of Classifier

Fig. 4.12 shows hardware architecture of our proposed classifier. Ten 16 bit comparators are required to compare results obtained from feature selection block with dynamic range as mentioned in table 4.1 obtained using training data. One 10 input OR gate is used to determine if any one of the input is out of the dynamic range, so as to classify the image as abnormal.

Table 4.5 gives the total number of gates required to calculate the hardware complexity of classifier in terms of logic gates. Total of 1289 gates are required to classify kidney images as normal or abnormal. From table 4.6 we can say that 6134 CMOS transistors are required to implement our

Table 4.5: Hardware complexity of classifier in terms of logic gates

Classsifier	NAND	AND	OR	NOR	XOR	NOT
16 Bit Comparator	-	640	160	160	-	320
10-Input OR gate	-	-	9	-	-	-
Total Gates	-	640	169	160	-	320

Table 4.6: Hardware complexity in terms of CMOS Transistors

Type of logic gate	No. of CMOS Transistors
AND	3840
OR	1014
NOR	640
NOT	640

classifier algorithm.

Thus from the above analysis, we see that a total of 6409 gates i.e. 28,554 transistors are required to implement our CAD algorithm which includes feature extraction and classification on hardware. Looking at the resources available in the recent computing platforms, this algorithm can be easily implemented.

Chapter 5

Abnormality detection using Automated Kidney detection algorithm

5.1 Block diagram of Kidney detection algorithm

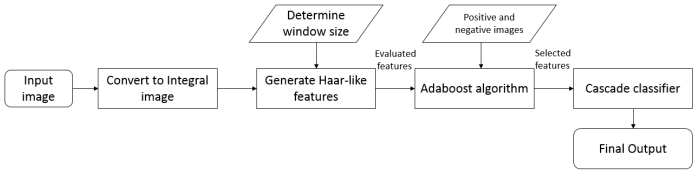

Figure 5.1: System architecture of kidney detection.

Kidney detection algorithm is based on Viola Jones technique. This algorithm is designed by giving kidney and non kidney ultrasound images as input and is trained to recognize a kidney in image. Later the designed algorithm can be used to detect kidney in any ultrasound image. According to this algorithm all the features of training data are calculated and are stored in a file, later features of new input image are evaluated and are compared with trained features to detect if there is kidney in image or not. This basic components corresponding to this algorithm include haar like features, integral image, Adaboost algorithm and cascade classifier.

Terminology

Image: Ultrasound B-mode image obtained from siemens ultrasound machine

Window: To denote detection rectangle where features are evaluated, size of window is less than or equal to size of image.

Haar-like features

Haar like features are derived from kernels [65], few of these kernels are shown in Fig. 5.2. The white region in kernel correspond to weight w_0=-1 and black region corresponds to w_1=+1. The value of these feature are then computed using the formula $f(x) = w_0 r_0 + w_1 r_1$, where $f(x)$ is the

response of a given Haar-like feature to the input image x, w_0 is the weight of the area r_0 and w_1 is the weight of the black area r_1. The number of pixels in areas r_0 and r_1 vary because the features are generated for various possible combinations and positions in a given window. These dimensions start from single pixel and extend upto the size of given window.

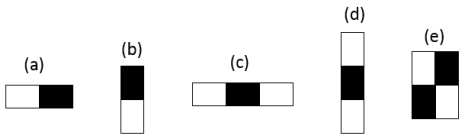

Figure 5.2: Kernels used to extract Haar like features in kidney detection algorithm.

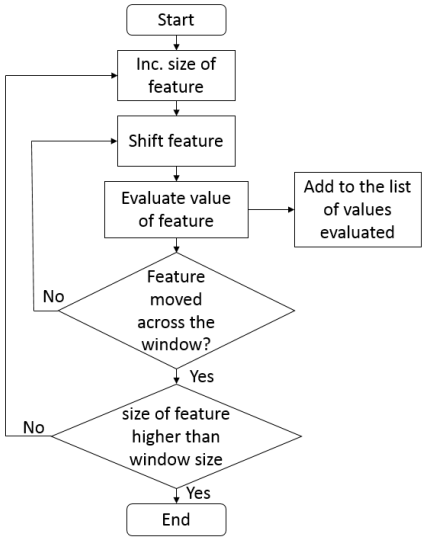

Figure 5.3: Flowchart to generate Haar-like features.

The features generated using kernels are independent of image content. The process of feature generation is explained as follows: considering kernel in Fig. 5.2(a) which is initially of two pixel column width (one pixel white and one pixel black) and feature value $f(x)$ is calculated. The kernel is shifted from top left of the image by one pixel and new feature value is calculated. Similarly kernel is then moved across the complete image until it reaches the right bottom of the image and all the feature values are calculated. Hence the features are evaluated hundreds of times as kernel moves across all the rows of image and every time new feature value is updated in features list. Later the kernel is increased to four pixel width (two white pixels and two black pixels) and the process is repeated to get new feature values. The process is repeated until the size of kernel reaches the size of the window. Considering all the variations of size, position of all the features, a total of 189,664 features were calculated for one kernel [62] in a window of size 24 $\times$ 24. Fig. 5.3 illustrates the flowchart for generating Haar-like features.

Integral Image

Computing sum of pixels in given area is computational intensive, hence intermediate representation of image is used to calculate the features rapidly and efficiently, this representation of image is called

as an integral image [66]. The conversion of image to integral image is based on the following formula

$$s(u,v) = s(u,v-1) + i(u,v)$$
$$i_1(u,v) = i_1(u-1,v) + s(u,v)$$

where u, v are the indices of the pixel, $s(u,v)$ is the cumulative sum of pixel values in a row (with initial conditions as $s(u,-1) = 0$, and $i_1(-1,v) = 0$), $i(u,v)$ is the pixel value of original image and $i_1(u,v)$ is the pixel value of integral image.

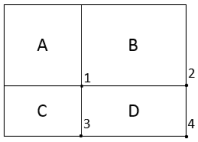

Figure 5.4: Sum of pixels in region D using four array reference.

In integral image, sum of all pixels under a rectangle can be evaluated using only the 4 corner values of the image. In Fig. 5.4 the value of the integral image at location 1 is the sum of the pixels in rectangle A, the value at location 2 is A + B, at location 3 is A + C, and value at location 4 is A + B + C + D. The sum of D can be evaluated as 4 + 1 - (2 + 3).

Adaboost algorithm

Adaboost is a machine learning algorithm which helps in finding only the best features among 180,000+ features [67], [68]. After evaluating the features obtained from Adaboost algorithm, weighted combination of these features are used in deciding whether given window has kidney or not. These selected features are also called as weak classifiers. The output of weak classifier is binary, either 1 or 0. 1 when the feature is detected in window and 0 when there is no feature in the window. Adaboost constructs a strong classifier based on linear combination of these weak classifiers.

$$F(x) = \alpha_1 f_1(x) + \alpha_2 f_2(x) + \alpha_3 f_3(x) + ...$$

where $F(x)$ is a strong classifier, $f_i(x)$ is a weak classifier and α_i is the weight corresponding to the error evaluated using classifier $f_i(x)$.

Adaboost starts with a uniform distribution of weights over training examples. Classifier with lowest weighted error (a weak classifier) is selected. Later the weights of the misclassified examples are increased and the process is continued till the required numbers of features are selected. Finally a linear combination of all these weak classifiers is evaluated and a threshold is selected. If the linear combination of new image in a given window is greater than this threshold it is considered as kidney being present, if it is less than threshold it is classified as nonkidney. Adaboost algorithm finds single feature and threshold that best separates the positive (kidney) and negative (nonkidney) training examples in terms of weighted error.

The process of selecting the features using Adaboost algorithm is shown in Fig. 5.5. Firstly, the initial weights are set for positive (with kidney) and negative (without kidney) examples. These weights are later normalized. Each classifier is used from 180,000+ features to determine the error, which in this case is to misclassify the presence of kidney in a window. If error is high, the training process ends, else the weights α_t are set to the selected linear classifier. The α_j are computed as

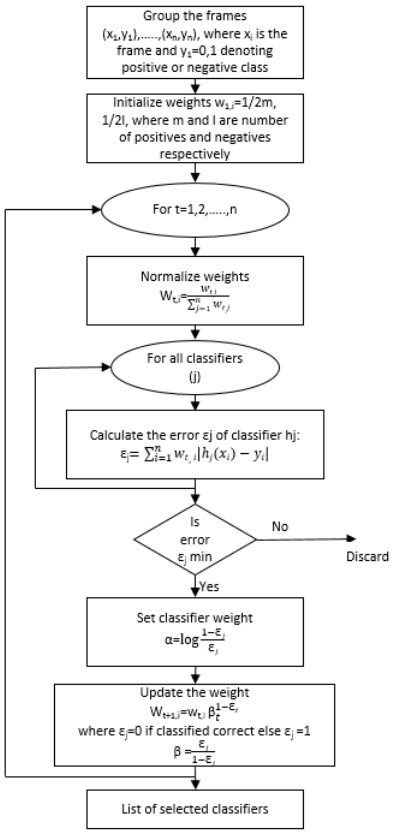

Figure 5.5: Flowchart of Adaboost algorithm.

$$\alpha_j = log\frac{1-\epsilon_j}{\epsilon_j}$$

where ϵ_j is the error occurred while classifying the images. Later the weights of the positive and negative examples are adjusted such that weights of the misclassified examples are boosted and weights to the correctly classified examples are not changed. Finally strong classifier is created which is a combination of weak ones weighted according to the error they had.

Cascade classifier

Strong classifier formed from linear combination of these best features is a computationally intensive procedure. Therefore a cascade classifier is used which consists of stages and each stage has a strong classifier [69]. So all the features are grouped into several stages where each stage has certain number of features along with strong classifier. Thus each stage is used to determine whether a kidney is present in given sub window. The block diagram of cascade classifier is shown in Fig. 5.6. A given sub window is immediately discarded if kidney is not present and is not considered for further stages. Cascade classifier works on the principle of rejection as majority of sub windows will be negative. It rejects many negatives at the earliest stage possible. This reduces the computational cost and hence kidney in the image can be detected at a faster rate.

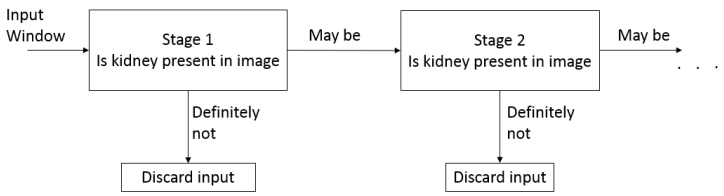

Figure 5.6: Block diagram of cascade classifier.

Reduction of Multiple detections

Multiple detections are a result of overlapping windows having same features as shown in Fig. 5.7. In this paper, we used two stage approach to reduce the multiple detection: In first stage, a window with size less than threshold of size 30×30 is dropped, threshold is selected based on the observations of several kidney images. In second stage, multiple windows with overlapping region of interest is merged into single window by averaging the coordinates of the window. The overlapping windows in image is determined if the union of two overlapping windows have more than 75% of pixels.

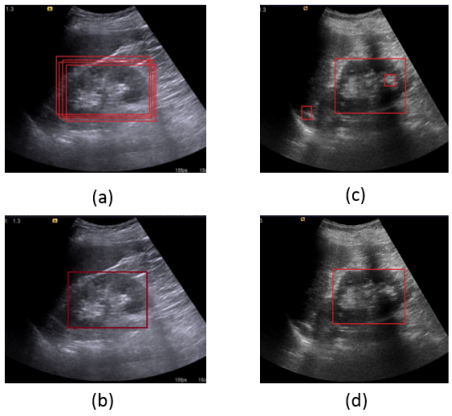

Figure 5.7: (a),(c) Multiple detection of kidney in ultrasound images, red boxes shows the region of interest for kidney. (b) Merging of Multiple detection in (a) to form single ROI. (d) Single ROI detection on (c) using threshold technique.

5.2 Abnormality detection

After detecting the kidney we developed algorithm based on SVM classifier to detect abnormality. Firstly ultrasound image is given to the system, where the system finds the presence of organ and detects Region Of Interest (ROI). Later ROI is segmented and its features are calculated. The calculated features are given to SVM classifier, based on its training set SVM classifier classifies whether the kidney is normal or abnormal. Finally after classification the image is sent to cloud along with priority that is abnormal images are sent with high priority and are diagnosed by doctor immediately.

5.2.1 Feature Extraction

After determining the ROI in ultrasound image, features are calculated to classify whether image is normal or abnormal. Initially we found 25 features are necessary to classify the kidney. Few features being redundant and does not play crucial role in classification. Removing the redundant features reduces the computational time. Later based on genetic algorithm we could reduce 25 features to only 6 features. The features that are considered for training the SVM classifier are mean, variance, standard deviation, skewness, kurtosis and entropy. These values are calculated as follows:

$$Mean, \mu = \frac{1}{MN} \sum_{i,j} I(i,j) \tag{5.1}$$

$$Variance, \sigma^2 = \frac{1}{MN} \sum_{i,j} (I(i,j) - \mu)^2 \tag{5.2}$$

$$Std.deviation = \sqrt{\sigma^2} \tag{5.3}$$

$$Kurtosis = \frac{1}{MN} \sum_{i,j} \frac{(I(i,j) - \mu)^4}{\sigma^4} \tag{5.4}$$

$$Skewness = \frac{1}{MN} \sum_{i,j} \frac{(I(i,j) - \mu)^3}{\sigma^3} \tag{5.5}$$

$$Entropy = \frac{1}{MN} \sum_{i,j} p(I(i,j)) logp(I(i,j)) \tag{5.6}$$

where $I(i,j)$ is the intensity value at i^{th} row and j^{th} column, $p(I(i,j)$ is the probability occurrence of intensity $I(i,j)$.

5.2.2 SVM Classifier

Support Vector Machine (SVM) is a linear classifier that is considered to be efficient for pattern recognition. kernels in SVM maps the feature vectors to higher-dimensional space to build an optimal linear classifier in the higher space so as to fit the training data [70]. The performance of SVM classifier with respect to different kernels is shown in Table. 5.1. Hence we used Radial Basis Function (RBF) kernel with variance 1. It can classify linearly non-separable features at lower dimensions to linearly separable at higher dimensional space. This reduces lot of computational complexity and can also provide better decision boundary as it is based on higher dimensional feature mapping.

Kernel	Accuracy(%)
Linear	82.35
RBF	92.94
Polynomial	85.29
MLP	87.05

Table 5.1: Accuracy of the proposed algorithm with respect to different kernels of SVM.

The SVM Classifier is trained with above mentioned features obtained from normal and abnormal images. Based on theses features SVM classifier can classify new image as either normal or abnormal.

When ultrasound image with kidney is given as input, kidney is detected from the image using kidney detection algorithm and its features are calculated. These features are fed as input to SVM classifier and image is classified.

5.3 Results

5.3.1 Database

Database is acquired using siemens ultrasound machine from 534 patients. These patients are in the age group of 14 to 65 years, including male and female gender. Images were obtained in all possible ways by changing parameters such as depth, time gain compensation, frequency. These variations can help in training kidney detection algorithm efficiently as all real time parameters are considered.

5.3.2 Metrics used for evaluating alogrithm

The performance of the proposed algorithm is evaluated by tabulating the confusion matrix. The metrics used are with reference to Fig. 5.8 is given below.

		Condition		
		Condition positive	Condition negative	
Test Outcome	Outcome positive	True Positive (TP)	False Positive (FP)	Positive predictive value
	Outcome negative	False Negative (FN)	True Negative (TN)	Negative Predictive Value
		Sensitivity	Specificity	

Figure 5.8: confusion matrix.

$$Sensitivity = \frac{TP}{TP + FN} \tag{5.7}$$

$$Specificity = \frac{TN}{TN + FP} \tag{5.8}$$

$$Positve\ Predictive\ Value = \frac{TP}{TP + FP} \tag{5.9}$$

$$Negative\ Predictive\ Value = \frac{TN}{TN + FN} \tag{5.10}$$

$$Accuracy = \frac{TP + TN}{Total\ test\ images} \tag{5.11}$$

Sensitivity measures the proportion of actual positives and specificity measures the proportion of actual negatives correctly identified as such respectively. Positive predictive value measures the efficiency of an algorithm to correctly identify normal kidneys and negative predictive value measures the efficiency of an algorithm to correctly identify negative images. In computer aided diagnosis, higher specificity is preferred as we do not want to classify abnormal image as normal. Specificity can be tolerable, as the loss occurred in classifying normal image as abnormal image is less.

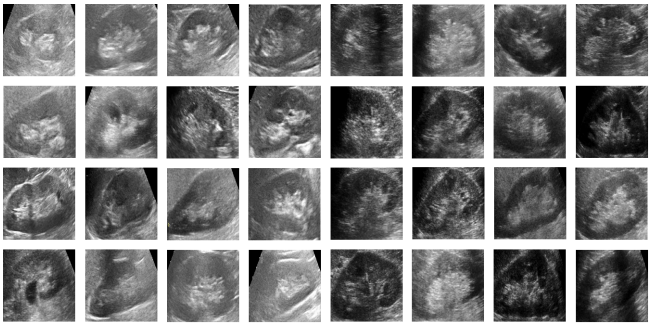

Figure 5.9: Some of the Kidney Images used in training Viola Jones algorithm.

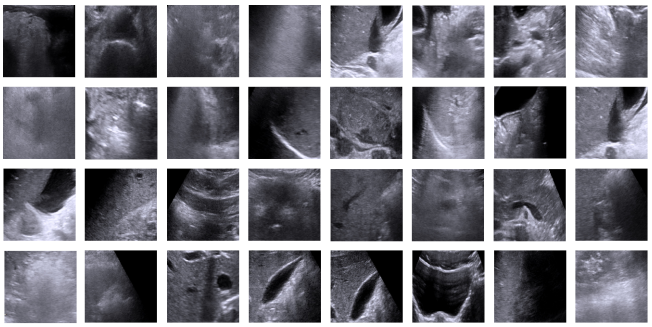

Figure 5.10: Some of the Images of negative training dataset used in Viola Jones algorithm.

For training the Viola Jones algorithm, 640 kidney images are used, out of which 320 are positive images with kidney as shown in Fig. 5.9 and 320 are negative images without kidney as shown in Fig. 5.10. Positive data set also include kidneys with abnormalities like cyst, infectious, stone etc., For training the Viola Jones algorithm, we manually marked the kidney images in the presence of sonographer.

The Viola Jones algorithm is initialized with following parameters: window enlargement in every step is set to 1.1, minimum size of initial window is set to 24 $\times$ 24 pixels. Size of the initial window was chosen to reduce the computational complexity, with small initial window detecting kidneys of big size becomes computationally intensive and big window size eliminates detection of small kidneys. Fig. 5.11 shows that employed Viola Jones algorithm with post processing could detect kidney with a positive predictive value of 91.25% for a training dataset of 160 images of which 80 are with kidney and 80 are without kidney. Fig. 5.12 shows some of the false positives that are detected in localizing kidney images.

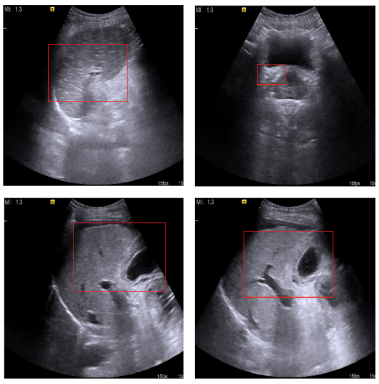

Figure 5.12: False Positives detected in localizing the kidney.

To detect the abnormality in the image after localization, we used 300 images to train the SVM classifier (with RBF kernel), of which 150 are normal cases and 150 are abnormal cases (consisting of stone, cyst). The proposed algorithm is tested with 90 normal kidney images and 80 abnormal images.

The performance of the proposed algorithm is tabulated in confusion matrix as shown in Fig.

		Predicted class of Ultrasound images		
		Images with kidney (80)	Images without kidney (70)	
Ultrasound Imaging test outcome	Images with kidney	73	5	Positive predictive value = 93.58%
	Images without kidney	7	65	Negative Predictive Value = 90.27%
		Sensitivity =91.25%	Specificity = 92.85%	

Figure 5.11: Results obtained by testing images with and without kidney.

		Patients with Kidney abnormality (as confirmed by sonographer)		
		Normal (90)	Abnormal (80)	
Kidney Imaging Test Outcome	Normal	85	7	Positive predictive value = 92.39%
	Abnormal	5	73	Negative Predictive Value = 93.58%
		Sensitivity =94.44%	Specificity = 91.25%	

Figure 5.13: Results obtained by testing normal and abnormal kidneys with proposed algorithm.

5.13. The proposed algorithm resulted with an accuracy of 92.94% (158 out of 170), sensitivity of 92.39 % and specificity of 93.58 %.

Fig. 5.14(a) shows the image of normal kidney obtained from siemens machine. Fig. 5.14(b) shows the image after segmentation. Segmentation is performed by system automatically without any human intervention. Based on segmented image, features are calculated and are given as input to SVM classifier with RBF kernel. The segmented image is classified normal as shown in Fig. 5.14(c).

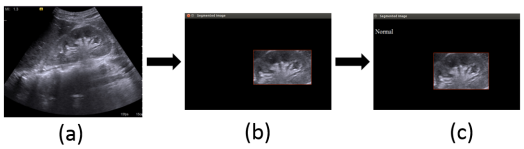

Figure 5.14: (a) Original image of normal kidney (b) Segmented kidney image (c) Classified kidney image.

Fig. 5.15(a) shows the image of abnormal kidney, cyst was the abnormality in this case as confirmed by doctor. Fig. 5.15(b) shows the segmented image obtained from our designed algorithm. Features were calculated form segmented image and is classified as abnormal by SVM classifier is shown in Fig. 5.15(c).

Experiments were performed on zed board that uses Xilinx zynq 7000 all programmable SOC running with Xillinux operating system at 667 MHz clock frequency. The simulations are verified using openCV platform. 5 stage training is used to train kidney detection algorithm so that it can detect the presence of kidney in ultrasound image. 13.96 seconds is taken to create feature list for Viola Jones algorithm. Viola Jones algorithm took 3.157 sec to detect the presence of kidney in

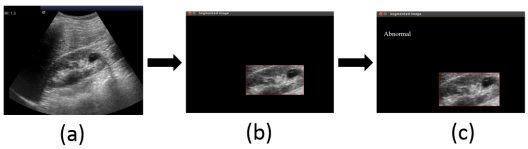

Figure 5.15: (a) Original image of abnormal kidney (b) Segmented kidney image (c) Classified kidney image.

image and 15.42 sec to determine if the kidney is normal or abnormal.

5.4 Conclusion

We developed a fully automated kidney diagnosis algorithm for ultrasound images. The Viola Jones algorithm is used for detecting and localizing the kidney. The Viola Jones algorithm results with multiple detection's of kidney in ultrasound image, which is solved by fixing hard threshold and merging techniques. The texture features are computed from detected window and SVM classifier is used for classifying the kidney image as normal or abnormal. Segmenting the image and transmitting only the ROI proves to be very efficient while transmitting data to cloud if the bandwidth of the channel is limited.

The automated diagnosis on kidney can be used as an additional tool for sonographers to make confident decisions. The simulations are verified on Xilinx Zed board, which has a capability of implementing entire ultrasound scanning system. The processor on Xilinx Zed board, can perform the computer aided diagnosis on the system and hence provides best solution for integrating both signal processing and diagnosis on a single system.

Chapter 6

Summary and Discussion

The two main focus areas of this work are (i) Backend implementation of FPGA platform (ii) Computer Aided Diagnosis for kidney. In this context, the thesis reports choice of compression techniques that best suite ultrasound imaging system, image enhancement technique to enhance the image clarity so as to not miss any critical information, kidney detection algorithm to localize the position of kidney, and reduction in the dimensionality of features required to detect whether the kidney is normal or abnormal. The algorithms are tested on various platforms and a large database to provide proof of concepts and support the claims made. In the course of these studies, several interesting insights were obtained. This chapter discusses future scope in this direction.

6.0.1 Backend Implementation of FPGA

We were able to present the FPGA based ultrasound backend system that would process the echo signals received from tissues. While processing we were able to develop envelope detection block using 32-tap FIR Hilbert transform, gamma compression block to compress the dynamic range, interpolation to reduce the blocking artifacts and finally image quality is enhanced using full scale contrast stretch to give a better contrast than traditional ultrasound systems. Various Compression techniques were assessed based on SSIM index. Gamma compression gave best results in terms of image clarity and can be implemented using Look Up Table (LUT) approach ensuring minimum hardware complexity. Implementation on FPGA reduces the cost of development and also provides a platform for the researchers to develop new algorithms and implement them which can lead to a new era of ultrasound imaging.

6.0.2 Computer Aided Diagnosis for Kidney

We proposed a fully-automated kidney abnormality detection system based on automated feature selection and supervised classification. The Viola Jones algorithm is used for localizing the kidney. The Viola Jones algorithm results with multiple detections of kidney in ultrasound image, which is solved by fixing hard threshold and merging techniques. The texture features are computed from detected kidney and SVM classifier is used for classifying the kidney image as normal or abnormal. The simulations are verified on Xilinx Zed board, which has a capability of implementing entire ultrasound scanning system. The processor on Xilinx Zed board, can perform the computer aided

diagnosis on the system and hence provides best solution for integrating both signal processing and diagnosis on a single system. Providing such information helps sonographers to suggest immediate precaution and also monitor disease progression. Thus the proposed technique aids prelimianry CAD for kidney on ultrasound systems.

References

[1] High, Whitney A., et al. "Gadolinium is detectable within the tissue of patients with nephrogenic systemic fibrosis." Journal of the American Academy of Dermatology 56.1 (2007): 21-26.

[2] Murphy, Sean W., Brendad J. Barrett, and Patrick S. Parfrey. "Contrast nephropathy." Journal of the American Society of Nephrology 11.1 (2000): 177-182.

[3] D. A. Christensen, "Ultrasonic Bioinstrumentation," Jonh Wiley and Sons, New York, 1988.

[4] J. A. Zagzebski, "Essentials of ultrasound physics," St Louis, Mo:Mosby, 1996.

[5] Mack, Michael J. "Minimally invasive and robotic surgery." Jama 285.5 (2001): 568-572.

[6] "bk ultraound [Online]. Available: http://www.ultrasonix.com/ultrasoundsystems/sonixtablet

[7] Yang, Min-Chun, et al. "Whole breast lesion detection using naive bayes classifier for portable ultrasound." Ultrasound in medicine and biology 38.11 (2012): 1870-1880.

[8] Sikdar, Siddhartha, et al. "A single mediaprocessor-based programmable ultrasound system." Information Technology in Biomedicine, IEEE Transactions on 7.1 (2003): 64-70.

[9] Kim, Gi-Duck, et al. "A single FPGA-based portable ultrasound imaging system for point-of-care applications." Ultrasonics, Ferroelectrics and Frequency Control, IEEE Transactions on 59.7 (2012): 1386-1394.

[10] Peng Zhang, "Programmable-logic and application-specific integrated circuits," Advanced Industrial Control Technology, First ed. Kidlington, UK:Elsevier Inc., ch. 6, sec. 2, pp. 224-226, 2010.

[11] Guyton, Arthur C. "Blood pressure control–special role of the kidneys and body fluids." Science 252.5014 (1991): 1813-1816.

[12] Statistics Division Ministry of Health and Family Welfare, Government of India, "Rural Health Statistics in India 2012" , March, 2012.

[13] Y. Kim, J. H. Kim, C. Basoglu, and T. C. Winter, "Programmable ultrasound imaging using multimedia technologies: A next-generation ultrasound machine," IEEE Trans. Inf. Technol. Biomed., vol. 1, no. 1, pp. 1929, 1997.

[14] V. Shamdasani, R. Managuli, S. Sikdar, and Y. Kim, "Ultrasound color-flow imaging on a programmable system," IEEE Trans. Inf. Technol. Biomed., vol. 8, no. 2, pp. 191199, 2004.

[15] S. Sikdar, V. T. Shamdasani, M. S. Lidstrom, K. W. Beach, and Y. Kim, "Low-cost detection and monitoring of coronary artery disease using ultrasound," in Proc. 1st Distributed Diagnosis and Home Healthcare Conf., 2006, pp. 5558.

[16] Y . M. Yoo, R. Managuli, and Y. Kim, "New multi-volume rendering technique for three-dimensional power Doppler imaging," Ultrasonics, vol. 46, no. 4, pp. 313322, 2007.

[17] U. Bae, M. Dighe, V. Shamdasani, S. Minoshima, T. Dubinsky, and Y. Kim, "Thyroid elastography using carotid artery pulsation: A feasibility study," in Proc. IEEE Ultrasonics Symp., 2006, pp. 614617.

[18] A. Agarwal, F. K. Schneider, Y. M. Yoo, and Y. Kim, "Image quality evaluation with a new phase rotation beamformer," IEEE Trans. Ultrason. Ferroelectr. Freq. Control, vol. 55, no. 9, pp. 19471955, 2008.

[19] F. K. Schneider, Y. M. Yoo, A. Agarwal, L. M. Koh, and Y. Kim, "New demodulation filter in digital phase rotation beamforming," Ultrasonics, vol. 44, no. 3, pp. 265271, 2006.

[20] Doi, Kunio. "Computer-aided diagnosis in medical imaging: historical review, current status and future potential." Computerized medical imaging and graphics 31.4-5 (2007): 198-211.

[21] Raja, K. Bommanna, M. Madheswaran, and K. Thyagarajah. "A hybrid fuzzy-neural system for computer-aided diagnosis of ultrasound kidney images using prominent features." Journal of Medical Systems, vol. 32.1, pp. 65-83, yr-2008.

[22] K. Divya, Vivek Akkala, R. Bharath, P. Rajalakshmi, and Abdul Mateen Mohammed. "FPGA based preliminary CAD for kidney on IoT enabled portable ultrasound imaging system." In e-Health Networking, Applications and Services (Healthcom), pp. 257-261. IEEE, 2014.

[23] Noble, J. Alison, and Djamal Boukerroui. "Ultrasound image segmentation: a survey." Medical Imaging, IEEE Transactions on vol.25.8, pp. 987-1010, yr. 2006

[24] Jun Xie; Yifeng Jiang; Hung-Tat Tsui, "Segmentation of Kidney From Ultrasound Images based on Texture and Shape Priors," Medical Imaging, IEEE Transactions on , vol. 24.1, pp.45-57, yr. 2005.

[25] Wu, Chia-Hsiang, and Yung-Nien Sun. "Segmentation of kidney from ultrasound B-mode images with textural based classification." Computer methods and programs in biomedicine, vol. 84.2, pp. 114-123, yr. 2006.

[26] Martn-Fernndez, Marcos, and Carlos Alberola-Lopez. "An approach for contour detection of human kidneys from ultrasound images using Markov random fields and active contours." Medical Image Analysis, vol. 9.1, pp. 1-23, yr. 2005.

[27] Ali, Asem M., Aly A. Farag, and Ayman S. El-Baz. "Graph cuts framework for kidney segmentation with prior shape constraints." Medical Image Computing and Computer-Assisted Intervention MICCAI Springer Berlin Heidelberg, pp. 384-392. yr. 2007.

[28] Prevost, Raphael, et al. "Kidney Detection and Segmentation in Contrast-Enhanced Ultrasound 3D Images." Abdomen and Thoracic Imaging. Springer US, pp. 37-67, yr. 2014.

[29] Viola, Paul, and Michael Jones. "Rapid object detection using a boosted cascade of simple features." Computer Vision and Pattern Recognition 2001. IEEE Computer Society Conference on. Vol. 1. IEEE, yr. 2001.

[30] Standard [online]. Available: http://ultrasonics.bioengineering.illinois.edu/data_patient.asp

[31] "zedboard [Online]. Available: http://zedboard.org/support/documentation/1521

[32] G. Wolberg, "Digital Image Warping." Los Alamitos, CA: IEEE Comput. Soc. Press, 1990.

[33] S. Sikdar, R. Managuli, and Y. Kim, "Programmable ultrasound scan conversion on a mediaprocessor-based system," in Proc. SPIE, vol. 4319, 2001, pp. 699711.

[34] J. O. Smith, "Mathematics of the Discrete Fourier Transform (DFT)," Center for Computer Research in Music and Acoustics (CCRMA), Department of Music, Stanford University, Stanford, California, 2002.

[35] A. V. Oppenheim and R. W. Schafer, "Discrete-Time Signal Processing." NJ: Prentice-Hall, Englewood Cliffs, 1989.

[36] S. Sukittanon, S. G. Dame, "FIR Filtering in PSoC with Application to Fast Hilbert Transform," Cypress Semiconductor Corp., Cypress Perform. (2005).

[37] Mawia Ahmed Hassan and Yasser Mostafa Kadah, "Digital Signal Processing Methodologies for Conventional Digital Medical Ultrasound Imaging System," IEEE Trans American Journal of Biomedical Engineering [Online], 3(1), 14-30, 2013. Available: http://journal.sapub.opr/ajbe

[38] Szabo, T. L., *"Diagnostic Ultrasound Imaging: Inside Out,"* Elsevier Academic Press: Hartford, Connecticut, 2004.

[39] R. C. Gonzalez, R. E. Woods, *"Digital Image Processing,"* Pearson Prentice Hall, Upper Saddle River, New Jersey, 2008

[40] Richard WD, Arthur RM, "Real-time ultrasonic scan conversion via linear interpolation of oversampled vectors," *Ultrason Imag.*, vol. 16, no. 2, 109-123, 1994.

[41] Standard [online]. Available: http://www.xilinx.com/products/silicon-devices/fpga/kintex-7

[42] Mohana Shankar, P., "A general statistical model for ultrasonic backscattering from tissues," Ultrasonics, Ferroelectrics, and Frequency Control, IEEE Transactions on , vol.47, no.3, pp.727,736, May 2000. doi: 10.1109/58.842062

[43] Szabo T. L., *"Diagnostic Ultrasound Imaging: Inside Out,"* Elsevier Academic Press: Hartford, Connecticut, 2004.

[44] V. Dutt and J. F. Greenleaf, "Adaptive speckle reduction filter for log-compressed B-scan images," *IEEE Trans. Med. Imag.*, vol. 15, no. 6, pp. 802-813, Dec. 1996.

[45] V. Dutt and J. Greenleaf, "Statistics of the log-compressed echo envelope," *J. Acoust. Soc. Amer.*, vol. 95, no. 3, pp. 3817-3825, 1996.

[46] Han, Young Seok, and Moon Gi Kang, "Image dynamic range compression by combining gamma-corrected images." *23rd Internation Technical conference on Circuits/Systems, computers and communications* (ITC-CSCC 2008), 2008.

[47] Y. Li, L. Sharan, and E. H. Adelson, Compressing and companding high dynamic range images with subband architectures," *ACM Transactions on Graphics*, vol. 24, no. 3, pp. 836-844, Aug. 2005.

[48] Standard [online]. Available: http://ultrasonics.bioengineering.illinois.edu/data patient.asp

[49] Z. Wang, A. C. Bovik, H. R. Sheikh and E. P. Simoncelli, "Image quality assessment: From error visibility to structural similarity," *IEEE Transactions on Image Processing*, vol. 13, no. 4, pp. 600-612, Apr. 2004.

[50] Z. Wang, E. P. Simoncelli and A. C. Bovik, "Multi-scale structural similarity for image quality assessment," IEEE Asilomar Conference Signals, Systems and Computers, Nov. 2003.

[51] David M. Rouse and Sheila S. Hemami, "Analyzing the Role of Visual Structure in the Recognition of Natural Image Content with Multi-Scale SSIM, " *Proc. Human Vision and Electronic Imaging* SPIE Vol. 6806, 2008.

[52] H. R. Sheikh, M. F. Sabir and A. C. Bovik, "A statistical evaluation of recent full reference image quality assessment algorithms", IEEE Transactions on Image Processing, vol. 15, no. 11, pp. 3440-3451, Nov. 2006.

[53] Wei, Dong, Umesh Rajashekar, and Alan C. Bovik "3.4 Wavelet Denoising for Image Enhancement."

[54] Wang, Fan, et al. "Synthetic aperture radar image segmentation using fuzzy label field-based triplet Markov fields model." IET Image Processing 8.12 (2014): 856-865.

[55] Dragotti, Pier Luigi, Giovanni Poggi, and Arturo RP Ragozini. "Compression of multispectral images by three-dimensional SPIHT algorithm." Geoscience and Remote Sensing, IEEE Transactions on 38.1 (2000): 416-428.

[56] Portilla, Javier, et al. "Image denoising using scale mixtures of Gaussians in the wavelet domain." Image Processing, IEEE Transactions on 12.11 (2003): 1338-1351.

[57] Hafizah, Wan Mahani, Eko Supriyanto, and Jasmy Yunus. "Feature extraction of kidney ultrasound images based on intensity histogram and gray level co-occurrence matrix." Modelling Symposium (AMS), 2012 Sixth Asia. IEEE, 2012.

[58] Oluleye, Babatunde, et al. "A genetic Algorithm-Based feature selection."British Journal of Mathematics and Computer Science (2014): In-Press.

[59] Eleyan, Alaa, and Hasan Demirel. "Co-occurrence matrix and its statistical features as a new approach for face recognition." Turkish Journal of Electrical Engineering and Computer Sciences 19.1 (2011): 97-107.

[60] Anjuli, Satyajit Anand. "2-Bit Magnitude Comparator Design Using Different Logic Styles." International Journal of Engineering Science Invention 2.1 (2013): 13-24.

[61] Acharyya, Amit, et al. "Coordinate rotation based low complexity ND FastICA algorithm and architecture." Signal Processing, IEEE Transactions on 59.8 (2011): 3997-4011.

[62] Viola, Paul, and Michael Jones. "Rapid object detection using a boosted cascade of simple features." Computer Vision and Pattern Recognition, 2001. CVPR 2001. Proceedings of the 2001 IEEE Computer Society Conference on. Vol. 1. IEEE, 2001.

[63] Prinosil, Jiri. "Local descriptors based face recognition engine for video surveillance systems." Telecommunications and Signal Processing (TSP), 2013 36th International Conference on. IEEE, 2013.

[64] Chu, Chengwen, et al. "Fully Automatic Segmentation of Hip CT Images via Random Forest Regression-Based Atlas Selection and Optimal Graph Search-Based Surface Detection." Computer Vision–ACCV 2014. Springer International Publishing, 2015. 640-654.

[65] Dalal, Navneet, and Bill Triggs. "Histograms of oriented gradients for human detection." Computer Vision and Pattern Recognition, 2005. CVPR 2005. IEEE Computer Society Conference on. Vol. 1. IEEE, 2005.

[66] Bradley, Derek, and Gerhard Roth. "Adaptive thresholding using the integral image." Journal of graphics, gpu, and game tools 12.2 (2007): 13-21.

[67] Osuna, Edgar, Robert Freund, and Federico Girosi. "Training support vector machines: an application to face detection." Computer Vision and Pattern Recognition, 1997. Proceedings., 1997 IEEE Computer Society Conference on. IEEE, 1997.

[68] Papageorgiou, Constantine P., Michael Oren, and Tomaso Poggio. "A general framework for object detection." Computer vision, 1998. sixth international conference on. IEEE, 1998.

[69] Lienhart, Rainer, Alexander Kuranov, and Vadim Pisarevsky. "Empirical analysis of detection cascades of boosted classifiers for rapid object detection." Pattern Recognition. Springer Berlin Heidelberg, 2003. 297-304.

[70] Suykens, Johan AK, and Joos Vandewalle. "Least squares support vector machine classifiers." Neural processing letters 9.3 (1999): 293-300.